UNIVERSITY OF THESSALY
SCHOOL OF ENGINEERING
DEPARTMENT OF MECHANICAL ENGINEERING

BUCKLING STRENGTH OF TUBULAR MEMBERS UNDER COMPRESSIVE LOADING USING FINITE ELEMENTS

by

STAMATINA STERGIOPOULOU

Submitted in partial fulfillment of the requirements for the degree of Diploma in Mechanical Engineering at the University of Thessaly

Volos, 2025

UNIVERSITY OF THESSALY
SCHOOL OF ENGINEERING
DEPARTMENT OF MECHANICAL ENGINEERING

BUCKLING STRENGTH OF TUBULAR MEMBERS UNDER COMPRESSIVE LOADING USING FINITE ELEMENTS

by

STAMATINA STERGIOPOULOU

Submitted in partial fulfillment of the requirements for the degree of Diploma in Mechanical Engineering at the University of Thessaly

Volos, 2025

Approved by the Committee on Final Examination:

Advisor	Dr. Spyros A. Karamanos, Professor, Department of Mechanical Engineering, University of Thessaly
Member	Dr. Costas Papadimitriou, Professor, Department of Mechanical Engineering, University of Thessaly
Member	Dr. Sotiria Chouliara, Lab Teaching Staff, Department of Mechanical Engineering, University of Thessaly

Acknowledgements

I would like to express my sincere gratitude to my supervisor, Dr. Spyros A. Karamanos, for his invaluable guidance, support, and encouragement throughout the course of this thesis.

I also extend my appreciation to the members of my thesis committee, Dr. Costas Papadimitriou and Dr. Sotiria Chouliara, for carefully reading my thesis and providing insightful comments and helpful suggestions.

I am especially thankful to Aristeidis-Georgios Stamou and Ilias Gavriilidis for their assistance in the simulations presented in Chapter 3 using Abaqus.

Finally, I would like to thank my family and everyone who supported me in my academic journey.

BUCKLING STRENGTH OF TUBULAR MEMBERS UNDER COMPRESSIVE LOADING USING FINITE ELEMENTS

STAMATINA STERGIOPOULOU

Department of Mechanical Engineering, University of Thessaly

Supervisor: Dr. Spyros A. Karamanos

Professor of Structural Mechanics

Abstract

Circular hollow sections (CHS) have been widely used in recent years, owing to their aesthetic appeal, unique properties and versatile applications. The present thesis investigates the buckling behavior of Normal Strength Steel (S355) tubular members under axial compression through Finite Element Analysis (FEA). A High Strength Steel (S700) is also examined to evaluate the effect of steel grade on buckling resistance. Varying slenderness ratios (λ) and diameter-to-thickness (D/t) ratios were examined. Two different modeling strategies were developed using Abaqus. Firstly, the tubular members were simulated as a two-dimensional model focusing on the global buckling response. Secondly, three-dimensional models were developed to account for local buckling and depict real-world structures more accurately. FEA models incorporated initial geometric imperfections and material nonlinearities to simulate realistic structural behavior. The global geometric imperfections were in the form of out-of-straightness, while the local imperfections were in the form of wrinkling. Several amplitudes were tested to assess imperfection sensitivity. A combined loading case, consisting of axial compression and internal pressure was additionally examined. The study demonstrates that the buckling strength of circular hollow section (CHS) members is highly influenced by global imperfections. When the amplitude increases, the buckling strength is reduced. Internal pressure combined with axial compression leads to significant reduction of buckling strength, particularly in low and moderate slenderness of members. High-strength steel (S700) exhibits lower sensitivity to imperfections than normal-strength steel (S355).

Keywords: CHS, Tubular Members, Initial Imperfections, Buckling Strength, Finite Element Analysis

ΔΟΜΙΚΗ ΕΥΣΤΑΘΕΙΑ ΣΩΛΗΝΩΤΩΝ ΜΕΛΩΝ ΥΠΟ ΘΛΙΨΗ ΜΕ ΤΗ ΧΡΗΣΗ ΠΕΠΕΡΑΣΜΕΝΩΝ ΣΤΟΙΧΕΙΩΝ

ΣΤΑΜΑΤΙΝΑ ΣΤΕΡΓΙΟΠΟΥΛΟΥ

Τμήμα Μηχανολόγων Μηχανικών, Πανεπιστήμιο Θεσσαλίας, 2025

Επιβλέπων Καθηγητής: Δρ. Σπύρος Α. Καραμάνος,

Καθηγητής Μηχανικής των Κατασκευών

Περίληψη

Οι Κυκλικές Κοίλες Διατομές (ΚΚΔ) έχουν γνωρίσει εκτεταμένη χρήση τα τελευταία χρόνια, λόγω της υψηλής αισθητικής τους, των ιδιαίτερων μηχανικών χαρακτηριστικών τους και της ευρύτητας εφαρμογών τους. Η παρούσα διπλωματική εργασία διερευνά τον λυγισμό σωληνωτών μελών από Χάλυβα (S355) υπό αξονική θλίψη με τη Μέθοδο Πεπερασμένων Στοιχείων. Παράλληλα, διερευνάται και η περίπτωση Χάλυβα Υψηλής Αντοχής (S700), προκειμένου να αξιολογηθεί η επίδραση της ποιότητας του χάλυβα στην αντοχή σε λυγισμό. Στο πλαίσιο αυτό, μελετήθηκαν διαφορετικοί λόγοι λυγηρότητας (λ) και λόγοι διαμέτρου προς πάχος (D/t). Αναπτύχθηκαν δύο διακριτές στρατηγικές μοντελοποίησης με τη χρήση του Abaqus. Στην πρώτη, τα σωληνωτά μέλη προσομοιώθηκαν ως δισδιάστατο μοντέλο εστιάζοντας στην ολική απόκριση λυγισμού. Στη δεύτερη, κατασκευάστηκαν τρισδιάστατα μοντέλα, τα οποία επέτρεψαν την αποτύπωση φαινομένων τοπικού λυγισμού και την προσέγγιση της πραγματικής συμπεριφοράς των κατασκευών με μεγαλύτερη ακρίβεια. Τα αριθμητικά μοντέλα περιέλαβαν αρχικές γεωμετρικές ατέλειες και μη-γραμμικότητες υλικού, ώστε να αναπαρασταθεί ρεαλιστικά η δομική απόκριση. Οι καθολικές γεωμετρικές ατέλειες εκφράστηκαν με τη μορφή απόκλισης από την ευθύτητα (out-of-straightness), ενώ οι τοπικές ατέλειες με τη μορφή πτυχώσεων (wrinkling). Εξετάστηκαν διάφορα πλάτη ατελειών προκειμένου να εκτιμηθεί η ευαισθησία των μοντέλων σε αυτές. Επιπλέον, μελετήθηκε και μια σύνθετη περίπτωση φόρτισης, η οποία συνδύαζε αξονική θλίψη και εσωτερική πίεση. Η μελέτη καταδεικνύει ότι η αντοχή σε λυγισμό των κυκλικών κοίλων διατομών (CHS) επηρεάζεται σε μεγάλο βαθμό από τις καθολικές ατέλειες. Όταν το πλάτος των ατελειών αυξάνεται, η αντοχή σε λυγισμό μειώνεται. Η εφαρμογή εσωτερικής πίεσης σε συνδυασμό

με αξονική θλίψη οδηγεί σε σημαντική μείωση της αντοχής σε λυγισμό, ιδιαίτερα σε μέλη χαμηλής και μέτριας λυγηρότητας. Ο χάλυβας υψηλής αντοχής (S700) παρουσιάζει μικρότερη ευαισθησία στις ατέλειες σε σύγκριση με τον χάλυβα κανονικής αντοχής (S355).

Λέξεις-κλειδιά: Κυκλικές Κοίλες Διατομές, Σωληνωτά Μέλη, Αρχικές Ατέλειες, Αντοχή σε λυγισμό, Μέθοδος των Πεπερασμένων Στοιχείων

Contents

LIST OF TABLES

LIST OF FIGURES

Chapter 1. INTRODUCTION

1.1 Motivation

Circular hollow sections (CHS) are widely used in modern structural systems, due to their distinct aesthetic appeal and superior mechanical behavior in various loading conditions. They have been widely used in a range of structural members such as columns, beams, arches, trusses and wind turbine towers [1]. The most common production methods for structural steel CHS are hot-rolling and cold-forming. There are several studies concerning global or local buckling of tubular members, but limited research has focused on the interaction of global and local buckling. The current study presents a numerical investigation into the stability of normal and high strength steel circular hollow section (CHS) beam-columns. Finite element (FE) models were developed towards this purpose using the general-purpose FE software Abaqus.

1.2 Introduction to Literature Review

This literature review presents an overview of previous research on the buckling behavior and compressive strength of circular hollow section (CHS) tubular members. It examines experimental, numerical, and analytical investigations that have explored the effects of manufacturing processes, geometric parameters, material properties, and imperfections on the overall performance of CHS columns. Emphasis is placed on studies addressing both cold-formed and hot-finished sections, as well as normal and high strength steel members.

The buckling behavior of CHS was examined by Ochi and Choo [2] who compared the two manufacturing processes, cold formed and hot finished with the existing Eurocode 3 (EC3) curves after several tests.

Recent studies have investigated the behavior of cold-formed CHS under axial compression, with particular emphasis on their susceptibility to different buckling modes. Dundu and Chabalala [3] tested 30 pin-ended CHS columns with varying diameter-to-thickness (D/t) and slenderness (KL/r) ratios. Their findings revealed that columns with lower D/t ratios failed by overall flexural buckling, whereas more slender sections with higher D/t ratios exhibited local ring-type buckling.

Fabricated CHS, which are produced by forming a steel sheet into a circular shape and welding longitudinally or spirally have been studied by Prion and Birkemoe [4] under combined axial load and bending. Similarly, Shi et al. [5] conducted experimental and numerical studies on welded circular tubes fabricated from 420 MPa high-strength steel, testing 24 pin-ended specimens with slenderness ratios between 20 and 60. Their results showed that most specimens failed by flexural buckling, with some interaction from local buckling, and that existing Chinese, European, and American column design curves tended to be overly conservative.

Pournara et al. [6] investigated the structural behavior and resistance of high-strength steel CHS members under axial compression and bending loading through experimental testing and numerical simulations. The influence of wrinkling as an initial imperfection was examined. High strength steel circular tubes under axial compression have also been examined by [7], [8], [9].

Meng and Gardner [10] conducted an experimental and numerical investigation into the flexural buckling of normal and high-strength steel CHS columns, whereas improvements to the existing Eurocode 3 design rules were proposed. The flexural buckling behavior of cold-formed stainless steel CHS columns has also been the focus of a comprehensive study by Buchanan et al. [11], where they examined different cross-section sizes (covering class 1 to class 4 sections) and a wide range of member slenderness. Local and global geometric imperfections were also incorporated in the finite element models. The authors proposed a new buckling curve that maintains the same format as the existing Eurocode provisions but with a reduced limiting slenderness (λ_0 = 0.20).

Hayeck et al. [12] conducted twelve buckling tests on S355 steel beam-columns with rectangular and circular hollow sections. The resistance of steel tubular beam-columns has been investigated and the Overall Interaction Concept is developed, which implies that the behavior of a steel member is influenced by the interaction between resistance and instability.

1.3 Thesis Organization

The remainder of this thesis is organized into four chapters 2-5. Specifically:

In Chapter 2, the geometry of the tubular members used in both the 2D and 3D models is presented, along with the corresponding material properties. Various types of imperfections incorporated in the numerical simulations are also described. Furthermore, the application of internal pressure as part of a combined loading case is discussed.

In Chapter 3, the numerical simulations carried out using the finite element software Abaqus are presented. The two modeling approaches, 2D and 3D, are described.

In Chapter 4, the numerical results obtained from the Finite Element Analyses are presented.

The conclusions of this study and suggestions for further research are presented in Chapter 5.

Chapter 2. PROBLEM FORMULATION

This chapter presents the fundamental setup used in the numerical simulation of the pipe under axial compression. It provides a detailed description of the geometric characteristics of the pipe for the 2D model. Subsequently, the material properties of the two steel grades used in this study, S355 and S700, are presented. Global geometric imperfections were also introduced. The internal pressure applied to the model was also discussed as part of the combined loading conditions. Finally, the 3D model geometric characteristics are described as well as the local-global imperfection that was applied in the simulations.

2.1 Tubular Members Geometry

The length of the tubular members is a variable in this study. Several lengths were tested, and the criterion was that the normalized slenderness $\bar{\lambda}$ should be in the range of $0.2 \le \bar{\lambda} \le 2.5$. Normalized slenderness is given by 2.1.

$$\bar{\lambda} = \frac{KL}{r}\sqrt{\frac{\sigma_y}{\pi^2 E}} \quad (2.1)$$

Where K is the effective length factor, affected by the boundary conditions applied to the model; r is the radius of gyration of the tubular cross section; E is the Young's modulus and σ_y is the yield stress. For simply supported members, K=1. The geometry data used for the models as a 2D beam-column are summarized in Table 2-1.

Table 2-1 Tubular members geometric properties

Outer Diameter D_o	323.85 mm	323.85 mm	323.85 mm
Thickness t	15 mm	7.5 mm	3 mm
D/t	21.59	43.18	107.95

2.2 Material Properties

2.2.1 Material Properties of Steel S355

The material used in this study is structural steel with the following mechanical properties, as shown in Table 2-2.

Table 2-2 Steel Properties

Yield Strength, σ_y	355 MPa
Young's modulus, E	200000 MPa
Poisson's ratio, ν	0.3

The steel's mechanical behavior can be approximated by a bilinear elastic-plastic stress-strain curve as defined in Annex C.6 of EN 1993-1-5 [13]. This curve consists of:

- An elastic region, where the stress-strain relationship is linear and defined by Hooke's law:

$$\sigma = E \cdot \varepsilon, \varepsilon \leq \varepsilon_y = \frac{\sigma_y}{E} \text{ (2.2)}$$

- A plastic region with linear strain hardening beyond the yield strain, described by the tangent modulus E_t:

$$\sigma = \sigma_y + E_t(\varepsilon - \varepsilon_y), \varepsilon > \varepsilon_y \text{ (2.3)}$$

Where ε and σ denote the engineering strain and stress, respectively. The tangent modulus E_t is taken as $E_t = E/1000$ to capture strain-hardening effects. However, Finite element software, such as Abaqus, requires the material plasticity input in terms of true stress σ_{true} and true plastic strain ε_{pl}. These are obtained from engineering stress and strain as presented in 2.4 and 2.5.

$$\sigma_{true} = \sigma_{eng}(1 + \varepsilon_{eng}) \text{ (2.4)}$$

$$\varepsilon_{true} = \ln(1 + \varepsilon_{eng}) \text{ (2.5)}$$

where σ_{eng} and ε_{eng} are the engineering stress and engineering strain, respectively.

The plastic strain ε_{pl} used in Abaqus is calculated by subtracting the elastic component, defined as the value of true stress divided by the Young's modulus, from the true strain:

$$\varepsilon_{pl} = \varepsilon_{true} - \frac{\sigma_{true}}{E} \text{ (2.6)}$$

The Engineering Stress-Engineering Strain curve is plotted in Figure 1 and the True Stress-Plastic Strain curve with the Abaqus input data is plotted in Figure 2.

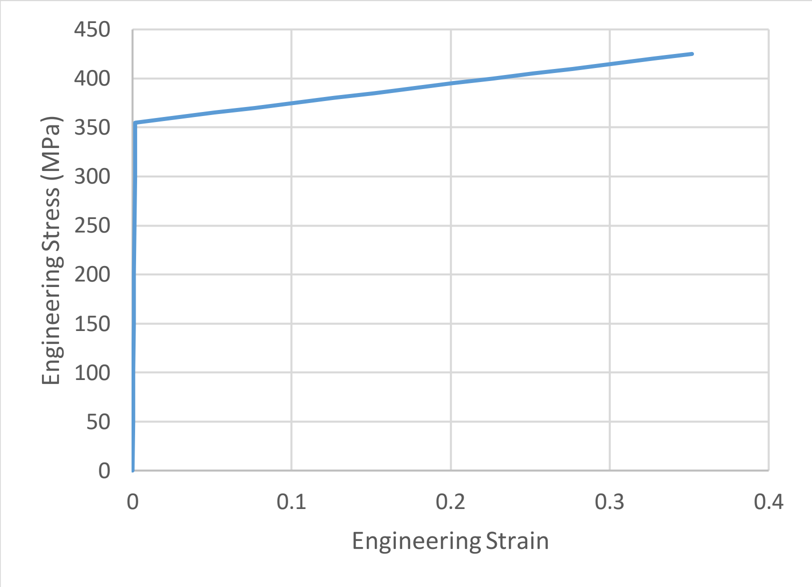

Figure 1: Engineering Stress-Engineering Strain curve

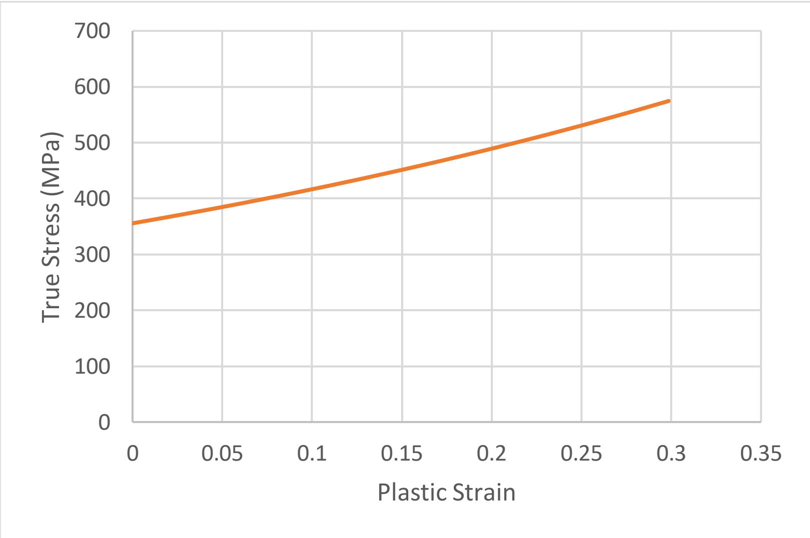

Figure 2: True Stress-Plastic Strain curve

2.2.2 Material Properties of High Strength Steel S700

A second type of material is tested, specifically a High Strength Steel (HSS), structural steel whose yield strength is greater than 460 MPa according to EN 1993-1-12 [14]. The mechanical properties are shown in the Table 2-3.

Table 2-3 High Strength Steel Properties

Yield Strength, σ_y	700 MPa
Young's modulus, E	200000 MPa
Poisson's ratio, v	0.3

The behavior of this steel grade is also approximated by a bilinear elastic-plastic stress-strain curve, as explained in Section 2.2.1. The same equations (2.2-2.6) are used to obtain both the Engineering Stress-Engineering Strain curve and the True Stress-Plastic Strain curve with the Abaqus input data. The resulting curves are plotted in Figure 3 and 4, respectively.

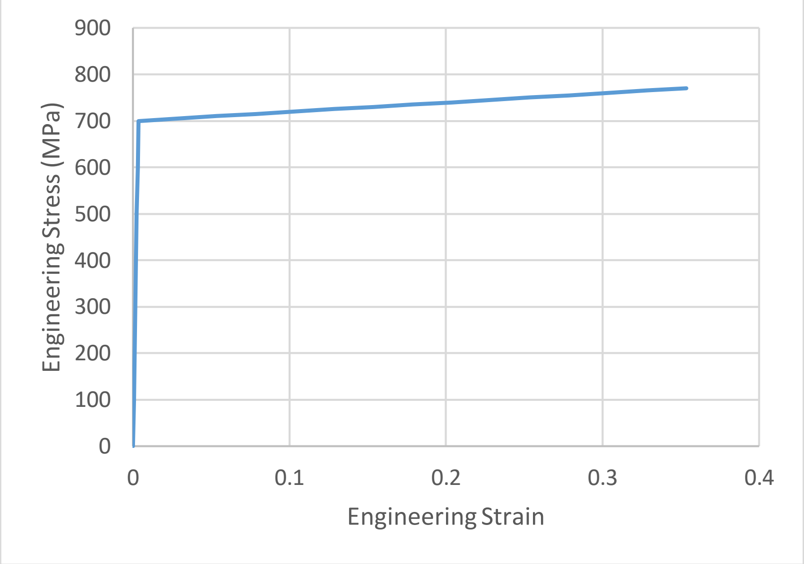

Figure 3: Engineering Stress-Engineering Strain Curve of HSS

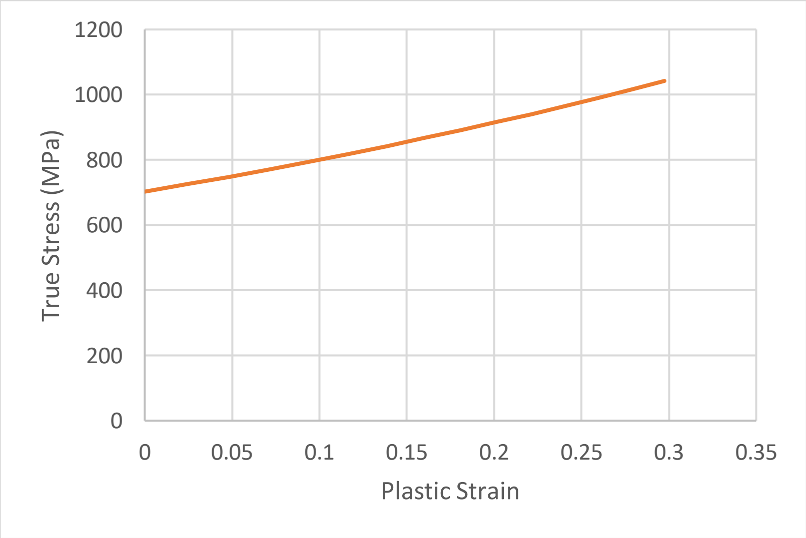

Figure 4: True Stress-Plastic Strain Curve of HSS

2.3 Global Imperfection Introduction and Amplitude Definition

In practice, circular hollow section (CHS) tubular members are never perfectly straight or geometrically ideal. Initial global geometric imperfections are typically represented as sinusoidal deviations along the member's axis, with amplitudes proportional to the member length. Geometric imperfections are usually a result of manufacturing processes, welding, transportation, and handling. In this thesis, the following amplitudes, L/5000, L/2500, L/1000 and L/500 were used as out-of-straightness global imperfections. L/1000 is a global imperfection amplitude that has been widely used in finite element models [15], [16].

2.4 Internal Pressure

The influence of internal pressure combined with axial compressive loading on the buckling strength of tubular members is investigated. Two pressure levels were considered: IP=17.272 MPa and IP=24.872 MPa corresponding to 50% of P_y and 72% of P_y respectively. Where P_y is the yield Pressure given by 2.7.

$$P_y = 2\sigma_y \frac{t}{D} \quad (2.7)$$

In this expression, D is the mean pipe diameter. It should be noted that most of the models were created considering only the axial compressive loading and no internal pressure effects.

2.5 Formulation of 3D Model

In this study, a three-dimensional finite element model was developed using shell elements to simulate the buckling behavior of circular hollow section (CHS) steel members subjected to axial compression. The CHS members were modeled with an outer diameter of 323.85 mm, and two wall thicknesses were considered: 7.5 mm (D/t=43.18) and 3.0 mm (D/t=107.95), representing stocky and slender profiles, respectively. According to EC3 [17] D/t=43.18 corresponds to Class 2 cross-section, while D/t=107.95 corresponds to Class 4 cross-section. To investigate the effect of member slenderness, three different lengths were analyzed: 4000 mm, 8000 mm and 12000 mm. The geometry data for the 3D Model simulation are summarized in the Table 2-4.

Table 2-4 Tubular members geometric properties of 3D Model

<table>
<tr><td>Length L</td><td colspan="2">4000 mm</td><td colspan="2">8000 mm</td><td colspan="2">12000 mm</td></tr>
<tr><td>Outer Diameter D_o</td><td colspan="6">323.85 mm</td></tr>
<tr><td>Thickness t</td><td colspan="3">7.5 mm</td><td colspan="3">3 mm</td></tr>
<tr><td>D/t</td><td colspan="3">43.18</td><td colspan="3">107.95</td></tr>
</table>

For consistency, the material properties used in the 3D modeling approach corresponded to those previously defined in Section 2.2.1.

2.6 Global and Local Imperfection

In this study, both global and local geometric imperfections were incorporated into the 3D finite element models to reflect real-world structural behavior more accurately. In several studies, global and local imperfections have been considered. In the present study, local imperfections have been introduced in the form of wrinkling caused by bending loading and then scaled as a fraction of thickness. Global imperfections are described in Section 2.3.

Chapter 3. FINITE ELEMENT ANALYSIS USING ABAQUS

This chapter presents the finite element modeling and analysis carried out using Abaqus [18] to investigate the buckling behavior of circular hollow section (CHS) steel members under axial compressive loading.

Two different approaches are presented, a 2D model and a 3D model, and the analysis procedure that was followed is described.

3.1 Abaqus Overview

Abaqus is a widely used commercial finite element analysis (FEA) software developed by Dassault Systèmes Simulia, known for its comprehensive capabilities in simulating complex structural behaviors under various loading conditions. Abaqus does not assume any specific unit system, therefore, all input parameters must maintain unit consistency throughout the analysis. The Abaqus units used in this study are listed in Table 3-1.

Table 3-1 Abaqus units

Quantity	Unit (SI mm)
Length	mm
Force	N
Stress	MPa

3.2 2D Model Formulation

To capture the structural behavior of the pipe while reducing computational cost, the geometry is idealized in this approach as a two-dimensional model within the Abaqus environment. It is noted that in this modeling strategy, the interest is in the global response of the tubular member rather than local buckling that can occur. The detailed procedure for creating the model in Abaqus is described in the following sections.

3.2.1 Part module

In the 2D Model approach, the tubular member is modeled as a wire. Many lengths were modeled to obtain the buckling curves and cover the slenderness range $0.2 \leq \bar{\lambda} \leq 2.5$. For illustration purposes, the length of the tubular member is chosen as L=4000 mm. Figure 5 and Figure 6 show how the Part is defined and sketched in Abaqus.

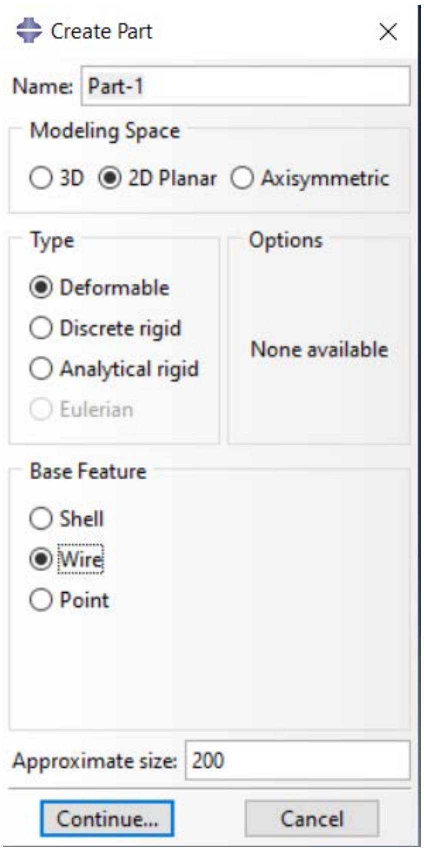

Figure 5: Part definition in Abaqus

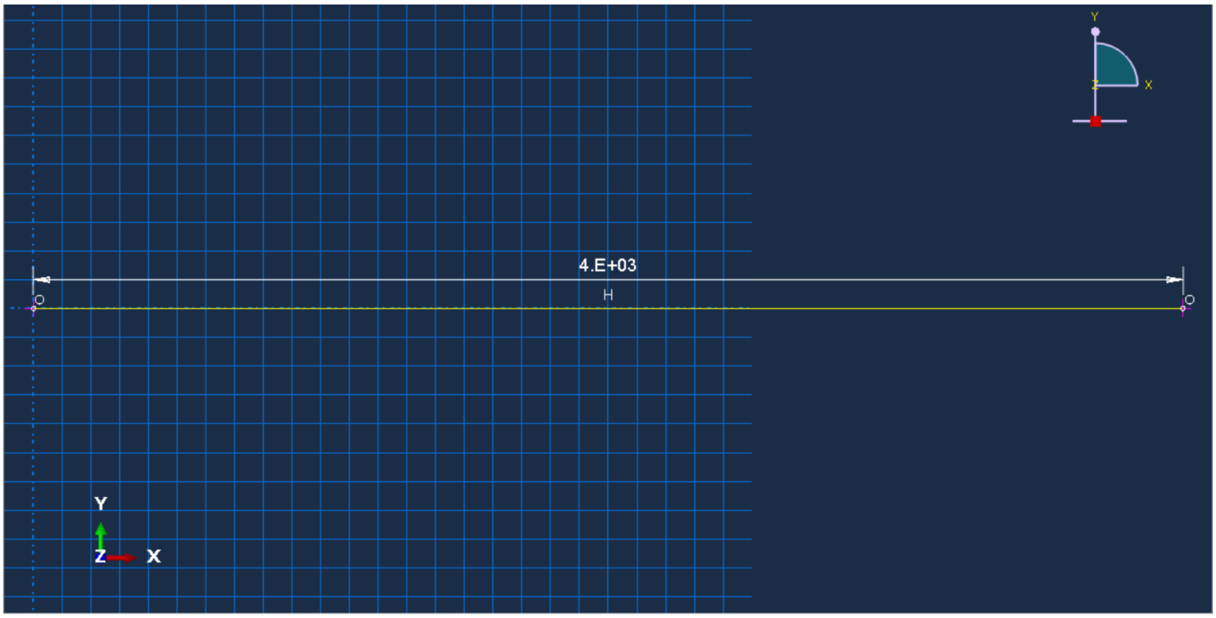

Figure 6: Part Sketch in Abaqus

3.2.2 Property module

In the property module the Material is defined as described in Section 2.2.1. In addition to that, the Beam Section is defined along with the Pipe Profile as shown in Figure 7.

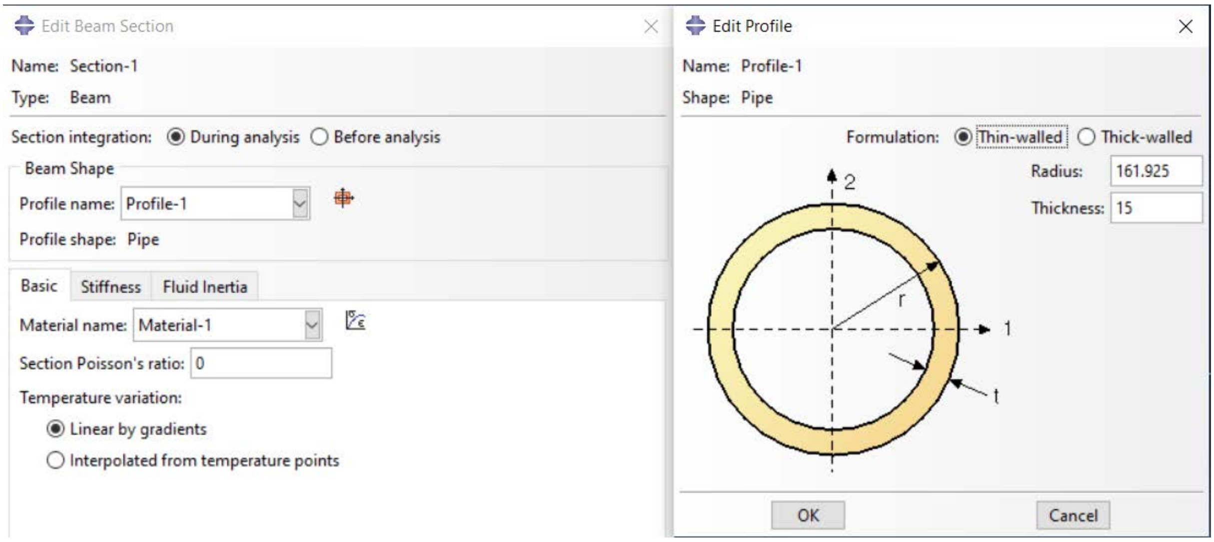

Figure 7: Beam Section and Pipe Profile in Abaqus

3.2.3 Mesh module

The tubular member was modeled using 400 uniformly spaced PIPE21 beam elements from the Abaqus/Standard library. PIPE21 is a 2-node, linear beam element formulated for two-dimensional (2D) planar analysis of pipe-like structures. PIPE21 elements are particularly well-suited for slender tubular members and allow the inclusion of internal pressure effects, which is not possible with standard beam elements such as B21.

3.2.4 Boundary Conditions

A pinned support was defined at the left end by constraining both U1 and U2, allowing rotation (UR3) to remain free. A roller support was modeled at the right end by restraining only U2, permitting axial compression and rotation. So, the boundary conditions are:

At x=0: $u_x = u_y = 0$

At x=L=4000 mm: $u_y = 0$

Figure 8: Boundary conditions in Abaqus

3.2.5 Analysis

A linear buckling eigenvalue analysis was initially conducted to determine the structure's critical buckling modes. The resulting first mode shape was scaled and applied as initial geometric imperfection in the model. A nonlinear finite element analysis was then performed firstly under axial compressive loading and secondly incorporating both internal pressure and axial compressive loading, to evaluate the structural response under realistic loading conditions with imperfections.

3.2.5.1 Linear Elastic Eigenvalue Buckling Analysis

A linear eigenvalue buckling analysis was performed in Abaqus using the Buckle step, with a unit compressive axial load of 1N applied at the end of the structure (x=L).The purpose of this step is to compute the critical buckling loads and the associated mode shapes under the reference loading condition. The analysis assumes linear elastic material behavior and does not account for geometric or material nonlinearities. The number of eigenvalues requested was 5, corresponding to the first 5 buckling modes. The first mode shape was subsequently used to introduce initial geometric imperfections in the nonlinear analysis, by scaling it with various imperfection amplitudes as a fraction of length. The load applied is shown in Figure 9 and in Figure 10 is shown the Buckle step formulation in Abaqus.

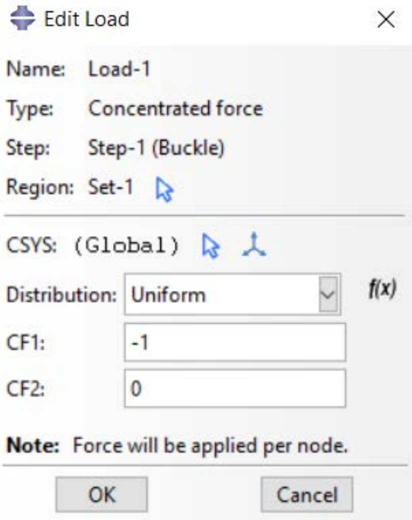

Figure 9: Load for Buckle Step

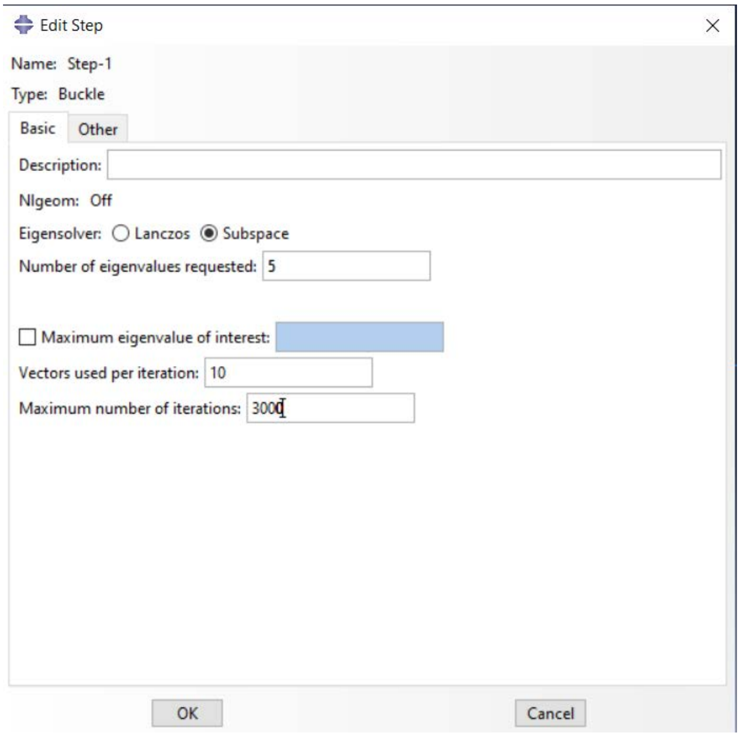

Figure 10: Buckle Step in Abaqus

3.2.5.2 Imperfection

Imperfections were introduced in the Abaqus model by applying a scaled eigenmode obtained from the linear buckling analysis. This approach follows the standard practice of representing the most critical mode shape to capture the sensitivity of the structure to initial deviations. The imperfection was introduced to the model through the input file keyword *IMPERFECTION. It is important to note that the *NODE FILE U keyword was added before *END STEP in the eigenvalue analysis input file, ensuring the mode displacements were saved to the results file. To summarize, the following line was included in the input file of the non-linear analysis to define the imperfection:

*IMPERFECTION, FILE=results_file, STEP=1

1, scale factor

Where results_file is the name of the job submitted to extract the eigenmodes,1 represents the first mode and scale factor is the amplitude of the imperfection. The amplitude is chosen as L/5000, L/2500, L/1000 and L/500 for different cases of length L. These values were chosen to represent a range from small manufacturing deviations to more severe geometric imperfections, allowing for assessment of imperfection sensitivity.

3.2.5.3 Static Step

In the first step, a Static General analysis was used to apply internal pressure to the inner surface of the pipe. Internal pressure was applied to the CHS steel tube using the Abaqus *DLOAD command with load type PI, which is specifically designed for internal pressure in pipe-type elements such as PIPE21. The effective diameter was also specified which is the inner diameter when internal pressure is applied. The nonlinear geometry option (NLGEOM=ON) was enabled to account for geometric nonlinearity due to large displacements and rotations and remains active during the subsequent step. The static step definition is shown in Figure 11. While the Internal Pressure definition and the visualization of it in Abaqus are shown in Figure 12 and Figure 13 respectively.

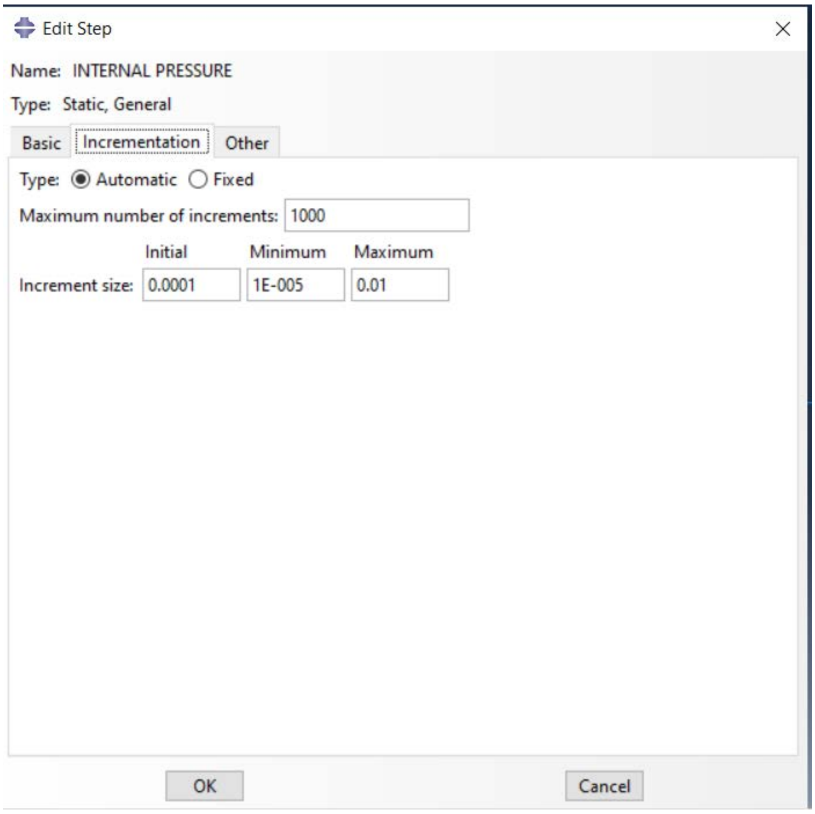

Figure 11: Static Step definition in Abaqus

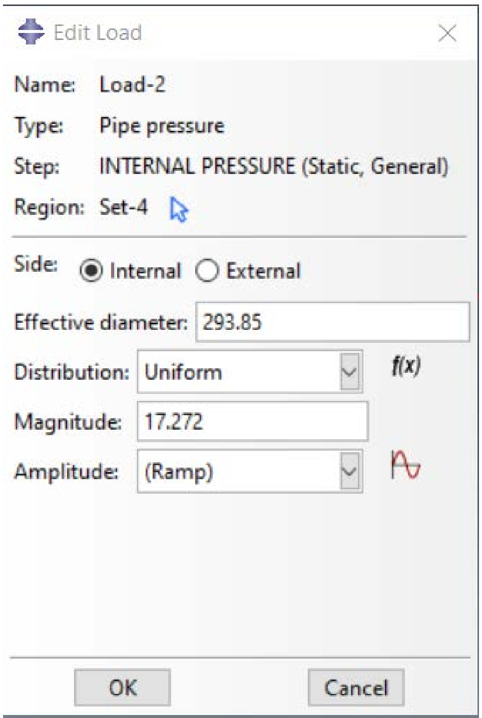

Figure 12: Internal Pressure definition in Abaqus

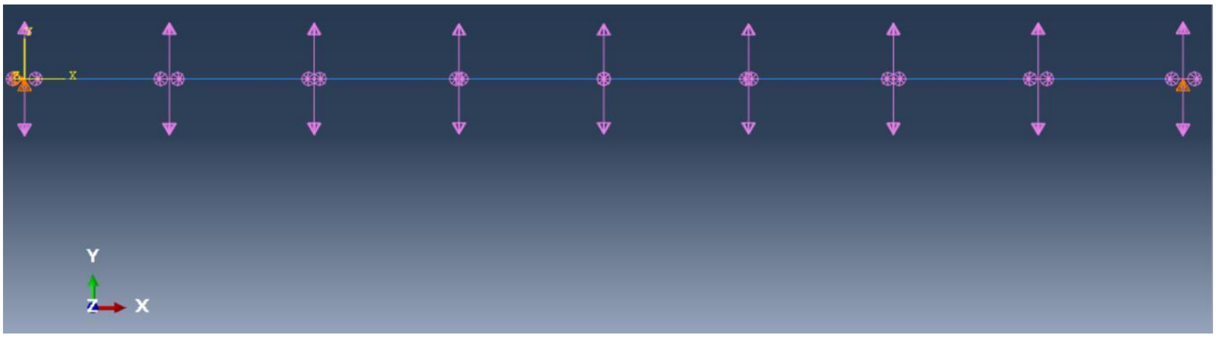

Figure 13: Internal Pressure visualization in Abaqus

3.2.5.4 Riks Step

The axial compressive load was applied using the modified Riks method (Static, Riks step) in Abaqus to perform a post-buckling analysis taking into consideration the imperfection of the structure. In the Riks step, loads carried over from previous steps and not redefined are regarded as “dead” loads, maintaining a constant magnitude throughout the analysis. The axial load defined in Riks step is called “reference” load and is entered as a unit load. Load application is governed by an arc-length control method, where all active loads are scaled proportionally using a load proportionality factor λ. At any point during the analysis, the actual load applied was:

$$P_{total} = \lambda \cdot P_{ref} \quad (3.1)$$

Where P_{ref} is the defined axial compressive load.

Figure 14 shows the Step definition window in Abaqus, where the arc-length incrementation parameters were configured for the Riks step.

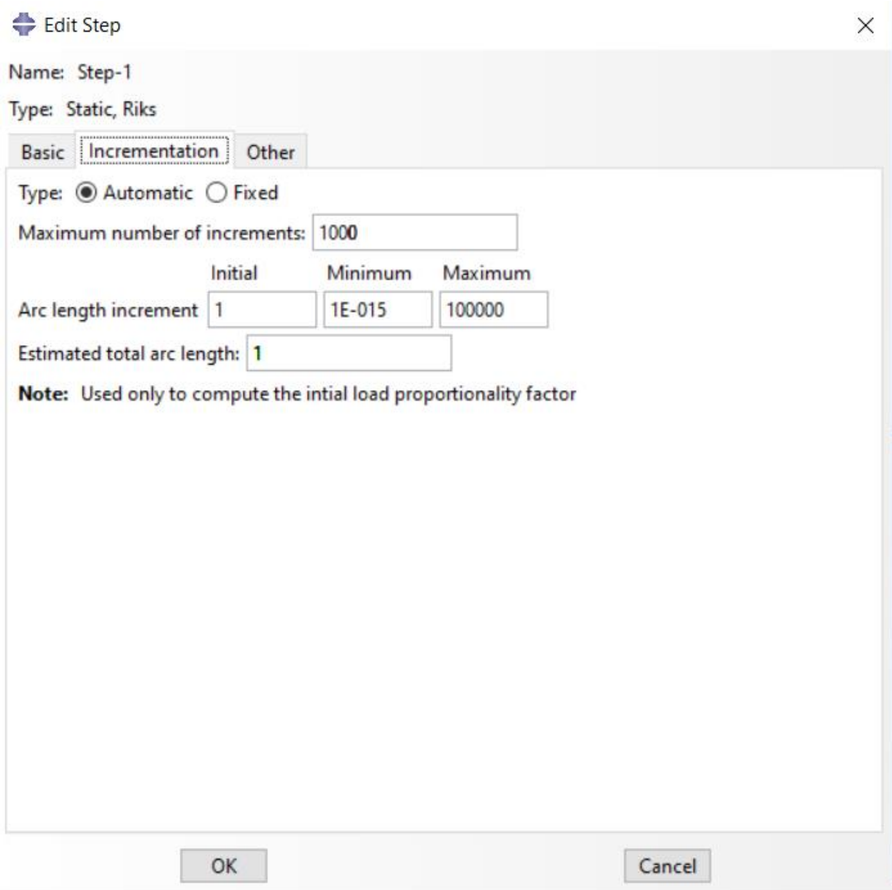

Figure 14: Riks step definition in Abaqus

3.3 3D Model

Following the description of the two-dimensional model, the three-dimensional model is now introduced. Although the 2D model provided useful initial insight into the pipe's axial compressive response, it cannot fully capture the three-dimensional deformation patterns and buckling modes that may arise. Therefore, a 3D model was developed to analyze the structure under axial compression, enabling a more realistic representation of global and local instability, including asymmetric and out-of-plane deformation effects that are not possible to simulate in a 2D framework.

3.3.1 Part Module

The tubular member was modeled as a 3D deformable shell part. A slightly curved geometry was created using the sweep feature with a three-point arc path, introducing a small geometric imperfection in the axial direction. The sweep path was defined by:

- Start point: (0,0)
- Midpoint: (L/2, -L/5000) = (2000, -0.8)

- End point: (L, 0) = (4000,0)

This shallow arc produces a small out-of-straightness along the tube's axis based on an imperfection ratio of L/5000, simulating manufacturing imperfections or initial geometric deviations, which are critical for realistic buckling behavior. The circular cross-section was defined using the outer radius 161.925 mm and then swept along the path to create the full 3D shell geometry. The section sketch is shown in the Figure 15, while the path sketch is shown in the Figure 16. Finally, in Figure 17 is shown the 3D part in Abaqus/CAE.

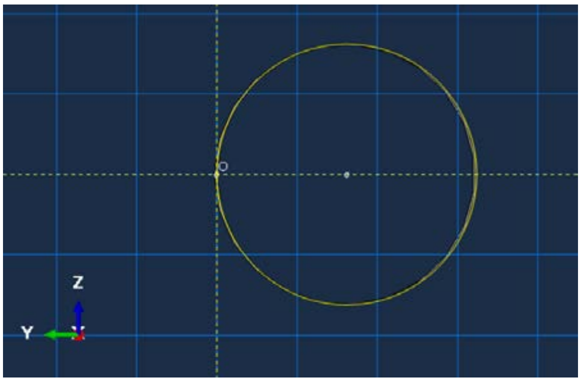

Figure 15: Circular section of part in Abaqus

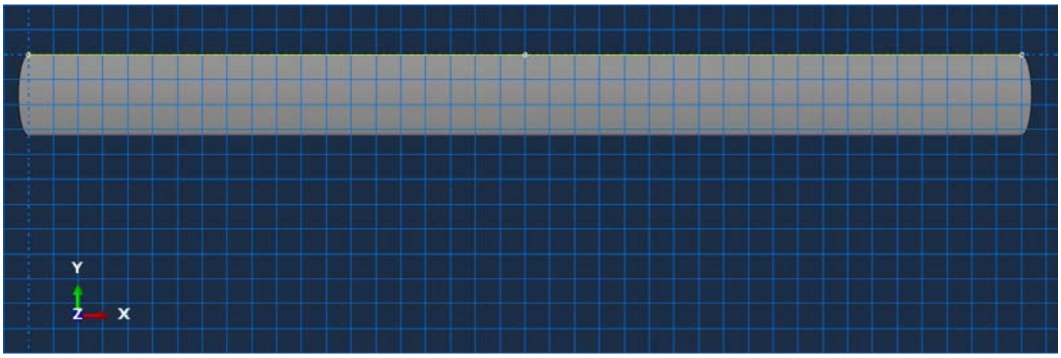

Figure 16: Path sketch of part in Abaqus

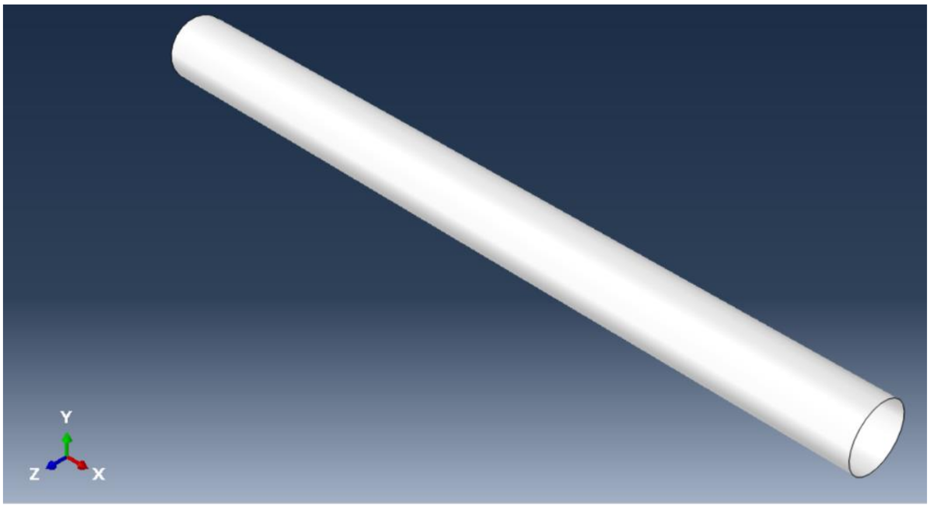

Figure 17: 3D Part in Abaqus

3.3.2 Property Module

In the Property Module the Material Properties are defined as described in Section 2.2.1. A homogeneous shell section is created, and the shell thickness is entered, in this case 7.5 mm. Then, the defined shell section was assigned to the entire geometry. Since the outer diameter of the tube was sketched in the part module, it is important to ensure that the shell section offset was set to position the shell mid-surface correctly within the wall thickness. For this model, the shell section offset was set to “Bottom” option in Abaqus. This offset shifts the mid-surface inward by half the shell thickness. Figure 18, shows the shell section with the thickness definition, while Figure 19 shows the section assignment and the shell offset definition.

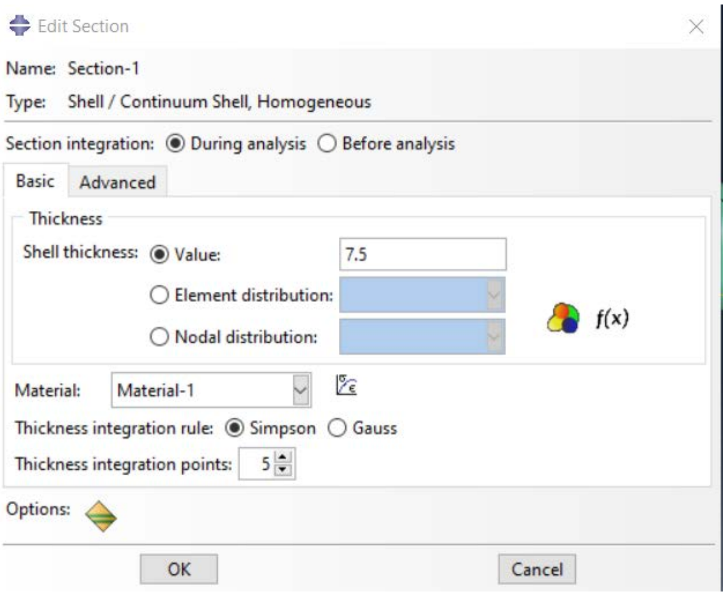

Figure 18: Shell section in Abaqus

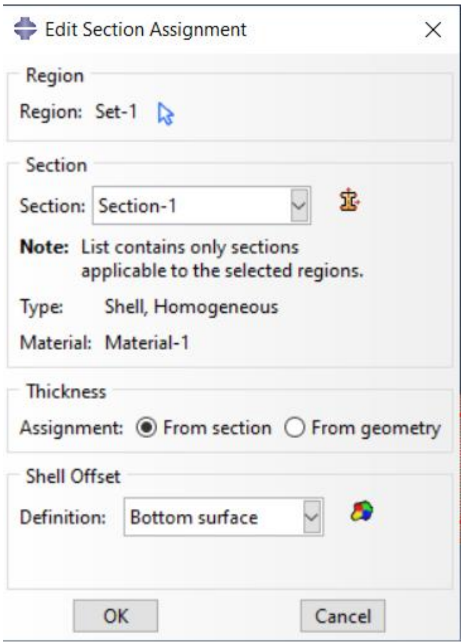

Figure 19: Section Assignment and Shell Offset definition in Abaqus

3.3.3 Mesh Module

The finite element mesh for the CHS steel tube was generated using S4R shell elements, which are 4-node, reduced-integration, shell elements suitable for modeling thin-walled structures with good accuracy and computational efficiency. This type of element has been successfully used in the accurate FE modeling of steel tubular columns [19], [20]. To enable local mesh refinement in the CHS member, three datum planes were created to partition the shell face:

- Two datum planes parallel to the YZ plane were positioned at x = 1676.15 mm and x = 2323.85 mm,
- One datum plane parallel to the XY plane was positioned at z = 0 mm.

Using these datum planes, the pipe's shell face was partitioned to define a refined mesh zone extending approximately one pipe diameter to the left and right of the mid-length along the pipe axis. This partitioning allowed applying a finer mesh in the critical central region, while a coarser mesh was used elsewhere to optimize computational efficiency. In the circumferential direction, the pipe was discretized using 80 elements. Along the axial direction (x-axis), element sizes were assigned using the Seed Edges function in Abaqus, with partitioning performed via datum planes to create distinct mesh regions:

- From x = 0 mm to x = 1676.15 mm, an element size of 15 mm was used.

- Between x = 1676.15 mm and x = 2323.85 mm, corresponding to a zone of interest around the pipe's mid-span, a refined element size of 7.5 mm was applied.
- From x = 2323.85 mm to x = 4000 mm, the element size returned to 15 mm.

Finally, mesh controls were assigned to all regions of the model and set to Structured. Figure 20 presents the final mesh applied to the tubular member.

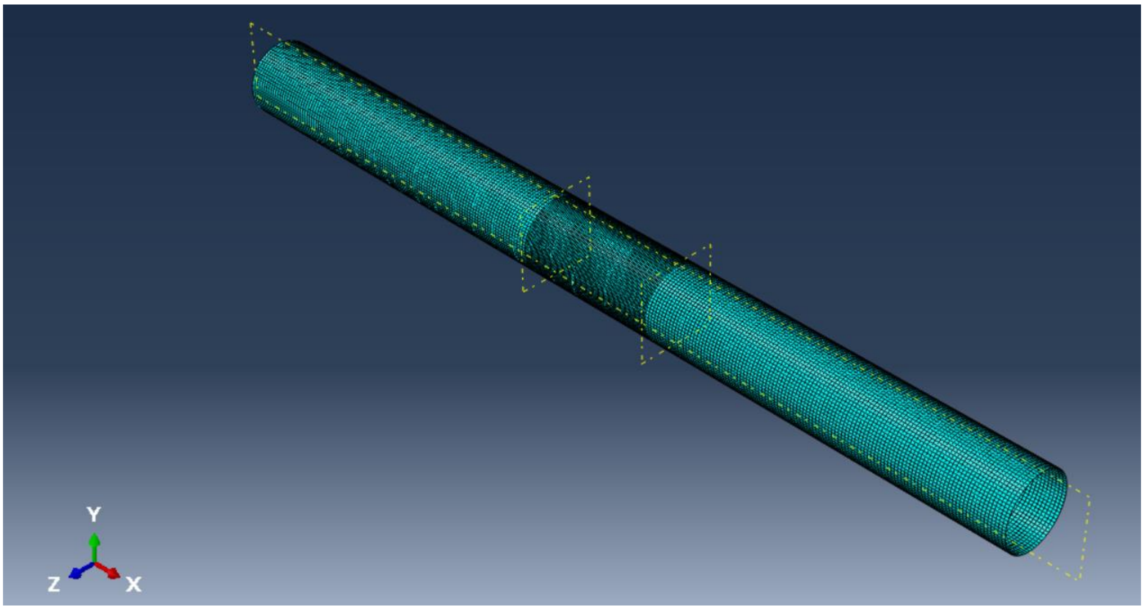

Figure 20: Non-uniform mesh of the tubular member where finer mesh is applied in the mid-span and coarser mesh near the ends

3.3.4 Interaction Module

To apply boundary conditions and loads uniformly to the pipe ends, kinematic coupling constraints were employed in the finite element model using Abaqus. In this approach, a reference point (RP) was defined at the geometric center of each pipe end, and a kinematic coupling was used to constrain the motion of all nodes on the corresponding end surface to this point. In Figure 21, the kinematic coupling constraint applied at the right pipe end is shown. At the left end of the pipe the kinematic coupling constraint was applied likewise.

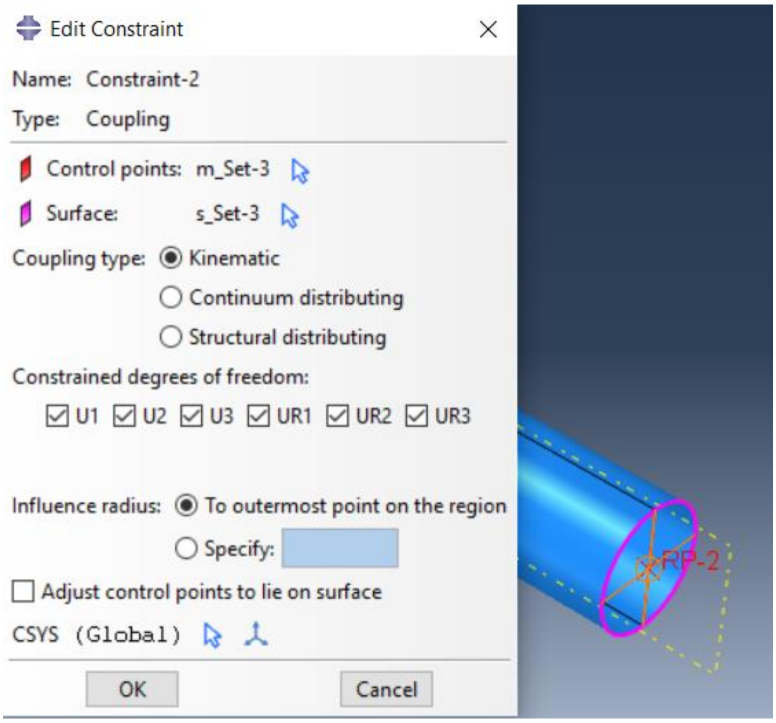

Figure 21: Kinematic coupling constraint applied to the right end of the pipe showing the RP and the associated slave surface

3.3.5 Boundary Conditions

The boundary conditions applied to the 3D model are the following. At the right end all translational degrees of freedom (U1, U2, U3) were constrained to prevent any rigid body motion. The rotational degrees of freedom about the X-axis (UR1) and Y-axis (UR2) were also restrained. At the left end of the pipe, only U1 was left free, to allow axial compressive loading. Finally, the rotational degrees of freedom about the X-axis (UR1) and Y-axis (UR2) were also restrained likewise. To summarize the boundary conditions are:

At x=0:

$$u_x = u_y = u_z = 0$$

$$\varphi_x = \varphi_y = 0$$

At x=L:

$$u_y = u_z = 0$$

$$\varphi_x = \varphi_y = 0$$

In Figure 22 and 23, the boundary conditions applied in Abaqus are shown.

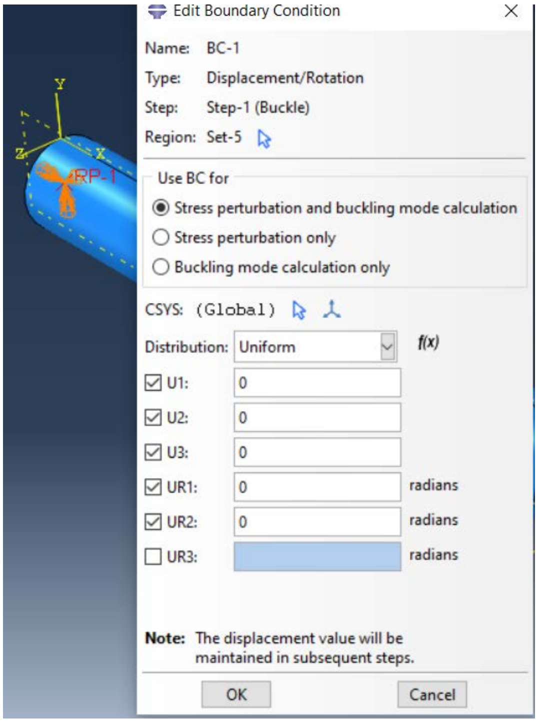

Figure 22: Boundary conditions at the right end of the pipe in Abaqus

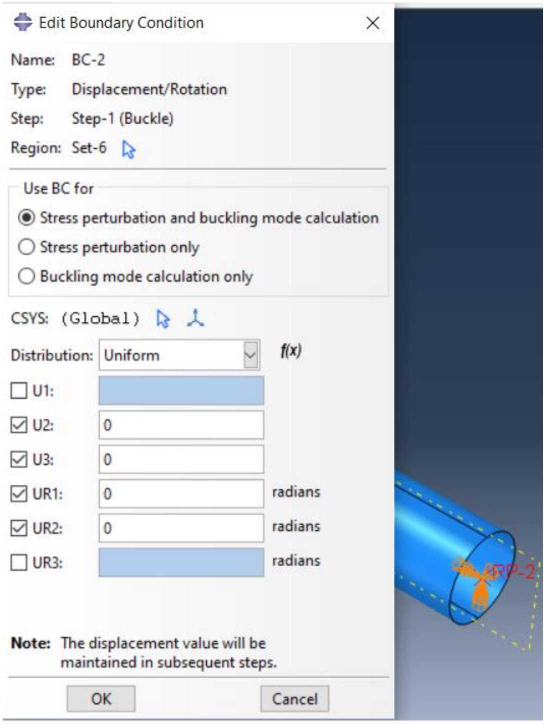

Figure 23: Boundary conditions at the left end of the pipe in Abaqus

3.3.6 Analysis

An eigenvalue analysis was first performed under pure bending loading conditions to identify the critical local wrinkling mode shape. The resulting first mode shape was afterwards scaled with different amplitudes as a fraction of thickness and applied as initial local imperfection in the model. Subsequently, a non-linear Riks analysis is conducted to calculate the structural behavior and the buckling strength of the tubular member under axial compressive loading, while considering both local and global initial imperfections.

3.3.6.1 Eigenvalue Analysis under Bending Loading Conditions

An eigenvalue analysis under bending was performed to obtain an initial geometric imperfection in the form of initial wrinkles along the tubular member. The number of eigenvalues requested was 5, corresponding to the first 5 buckling modes. However, only the first mode was subsequently scaled for the introduction of imperfection in the model. The load applied in Abaqus to observe wrinkling, is Moment in the z-direction, at x=0: CM3=-1 and at x=L: CM3=1.

In Figure 24 and 25, the Moment applied in Abaqus are shown. While in Figure 26, the visualization of Moment application in the Abaqus environment is shown.

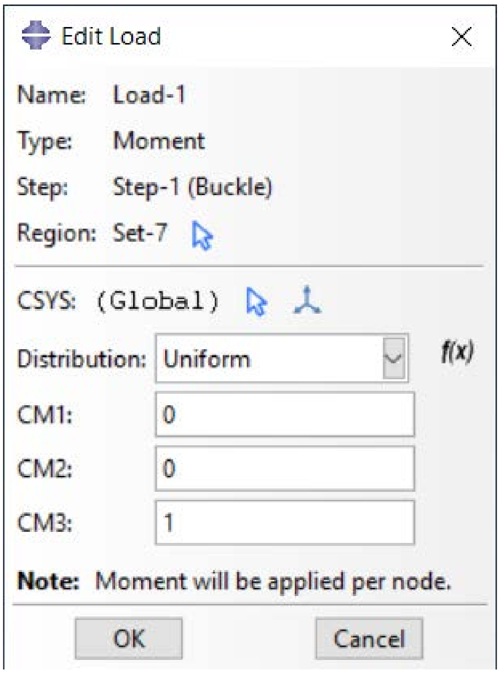

Figure 24: Moment applied at the left end of the pipe

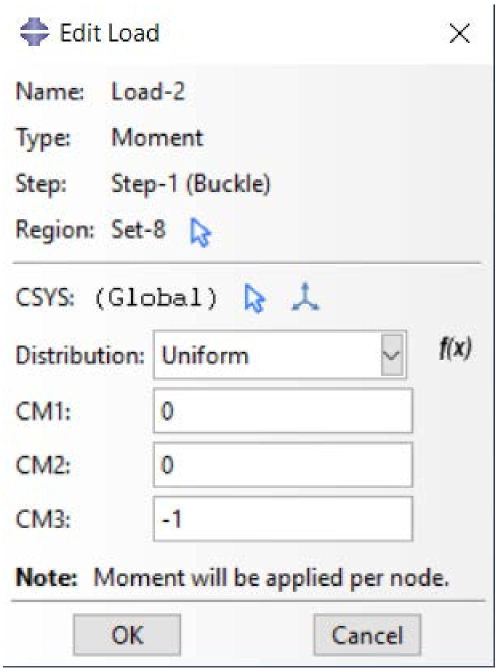

Figure 25: Moment applied at the right end of the pipe

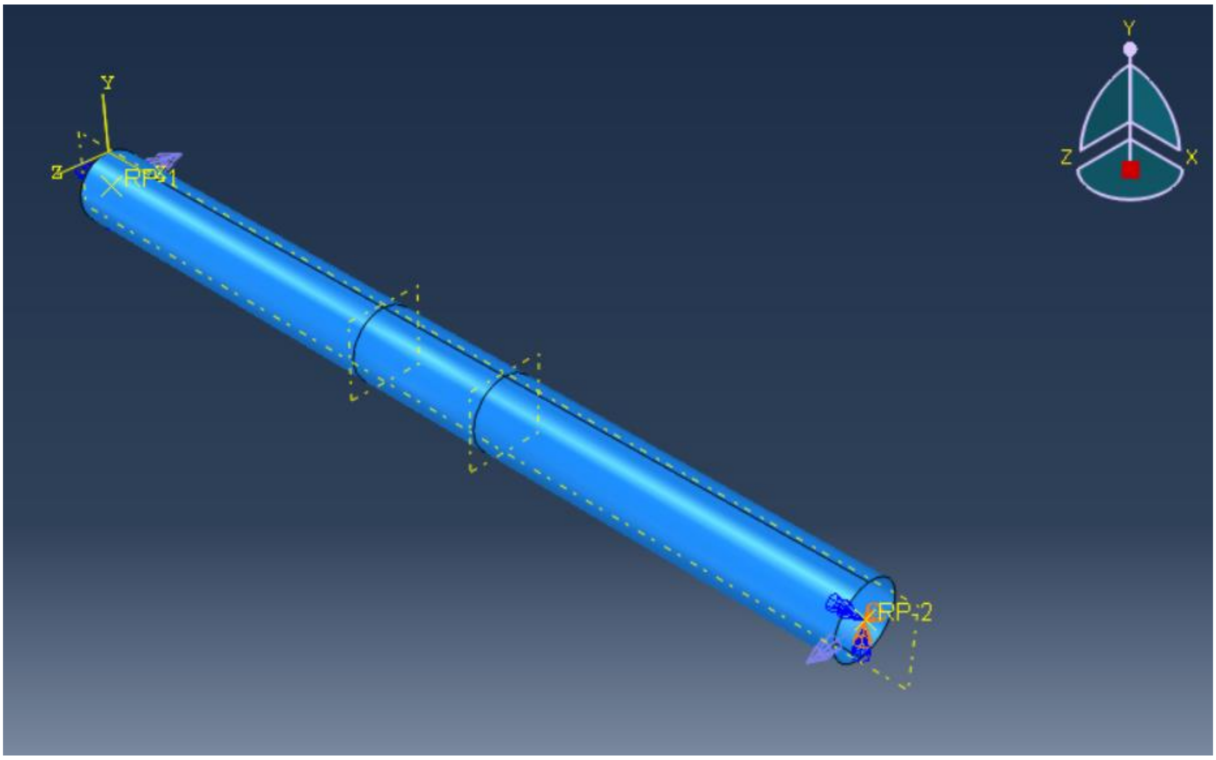

Figure 26: Moment application in Abaqus

3.3.6.2 Initial Local Geometric Imperfection

Local imperfections in the form of wrinkles along the tube were introduced in the Abaqus model by applying a scaled eigenmode obtained from the eigenvalue analysis. The imperfection was introduced to the model through the input file keyword *IMPERFECTION. To summarize, the following line was included in the input file of the non-linear analysis to define the imperfection:

*IMPERFECTION, FILE=results_file, STEP=1

1, scale factor

Where results_file is the name of the job submitted to extract the eigenmodes,1 represents the first mode and scale factor is the amplitude of the imperfection. The amplitude is chosen as a fraction of thickness and specifically, 0.05t, 0.1t, and 0.15t. These values of amplitude were in accordance with those obtained in [6] which varied from 1% to 20% of thickness of the member.

3.3.6.3 Non-linear analysis-Riks Step

To accurately capture the post-buckling behavior of the structure under axial compressive loading, a nonlinear static analysis was performed using the modified Riks method in Abaqus. This method uses the load as an additional parameter and it solves simultaneously for loads and displacements. The equation of Load in every increment is described in Section 3.2.5.4.

Chapter 4. NUMERICAL RESULTS

In this Chapter, the numerical results from the Abaqus finite element analyses are presented for both 2D and 3D model assumptions.

4.1 2D Model Results

In the 2D Model results, the influence of initial global imperfection amplitude, the effect of Internal Pressure combined with axial compressive loading, the influence of thickness and the influence of different steel grades, normal S355 and high strength steel S700 are tested.

In Figure 27, the first eigenmode from the eigenvalue buckling analysis for L=4000 mm is shown. In Figure 28, the buckled shape of a tubular member of length L=4000 mm, t=15 mm, global imperfection amplitude L/5000 is shown.

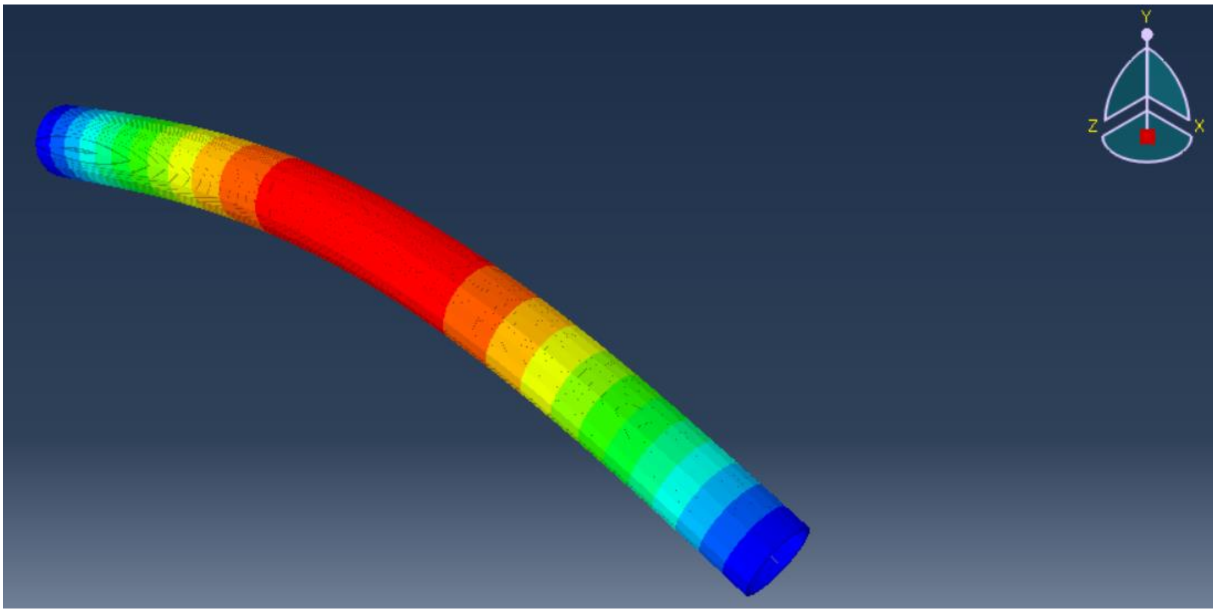

Figure 27: First eigenmode from Linear Buckling Analysis for L=4000 mm, which is later scaled and superimposed as an initial imperfection in the non-linear Finite Element Analysis

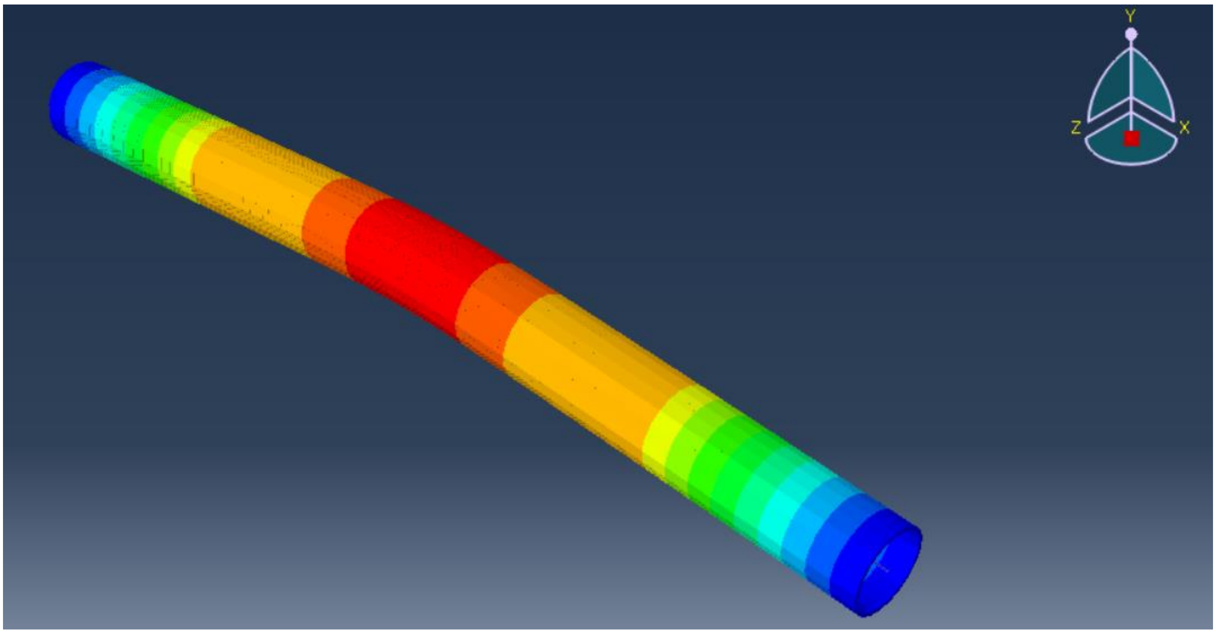

Figure 28: Buckled shape of a tubular member of length L=4000 mm, t=15 mm, global imperfection amplitude L/5000, exhibiting Euler-type buckling

4.1.1 Influence of Initial Global Imperfection Amplitude

Assuming t=15 mm and σy=355 MPa, four different amplitudes as a fraction of member length L are tested. Specifically, the influence of the global imperfection amplitudes of out-of-straightness L/5000, L/2500, L/1000 and L/500 are presented in a diagram of Normalized maximum Stress-Normalized Slenderness. The diagram is plotted in Figure 29.

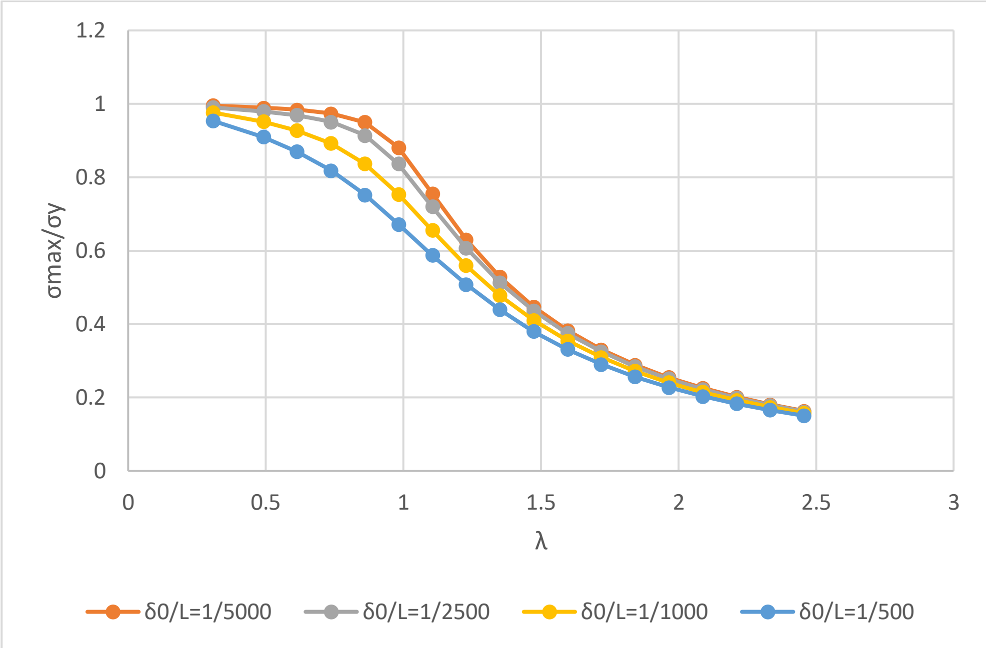

Figure 29: Normalized maximum Stress-Normalized Slenderness curves for L/5000, L/2500, L/1000, L/500

The parametric study demonstrates that initial geometric imperfections significantly affect the axial compressive capacity of CHS members. For low λ, all imperfection amplitudes resulted in similar stress capacities, indicating that yielding governed the response. As member slenderness increases, the impact of imperfections is more pronounced. Members with imperfection amplitude L/500 exhibit significantly reduced strength compared to those with imperfection amplitude L/5000. At intermediate level of member slenderness, imperfections have a much bigger impact because both yielding and buckling are interacting. So, as initial global imperfection amplitude increases, the strength of the members is reduced. For very slender CHS members, the main concern under axial compression is elastic buckling, not material yielding. The effect of initial imperfections becomes less critical as the member slenderness λ approaches 2-2.5. This happens because slender columns already have low buckling strength, so adding imperfections doesn't significantly lower the capacity any further.

4.1.2 Influence of Internal Pressure

Again, for t=15 mm and σy=355 MPa, but for two imperfection amplitudes, L/2500 and L/1000 the influence of Internal Pressure along with the axial compressive loading is tested. Three levels of Internal Pressure are presented: 0, 17.872 MPa (0.5Py) and 24.872 MPa (0.72Py). For the two different imperfection amplitudes, L/2500 and L/1000, the Normalized maximum Stress-Normalized Slenderness curves are plotted in Figure 30 and Figure 31 respectively.

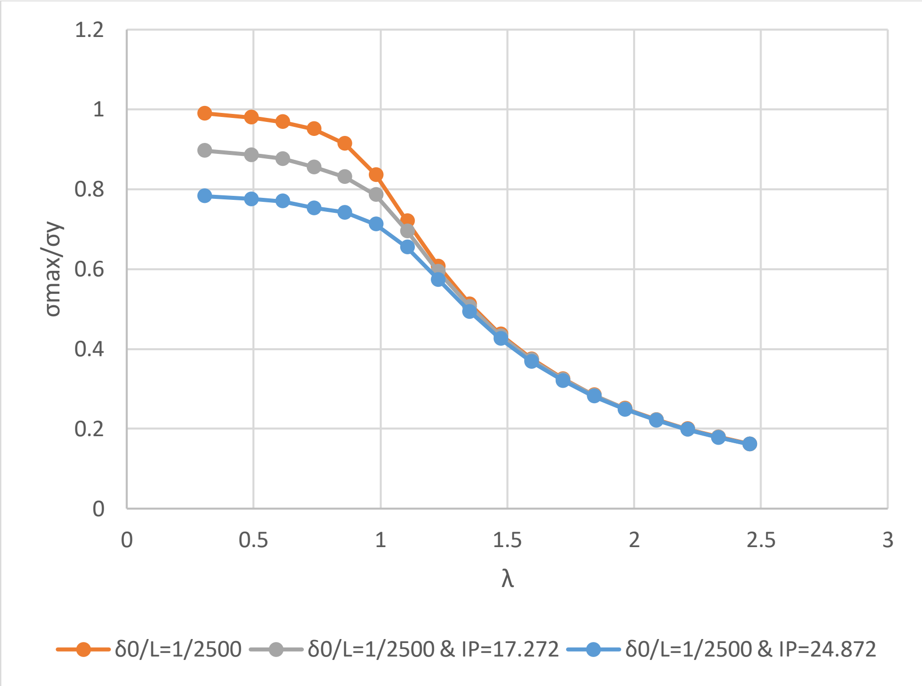

Figure 30: Normalized maximum Stress-Normalized Slenderness for imperfection amplitude L/2500 and IP=0, 17.272MPa and 24.872MPa

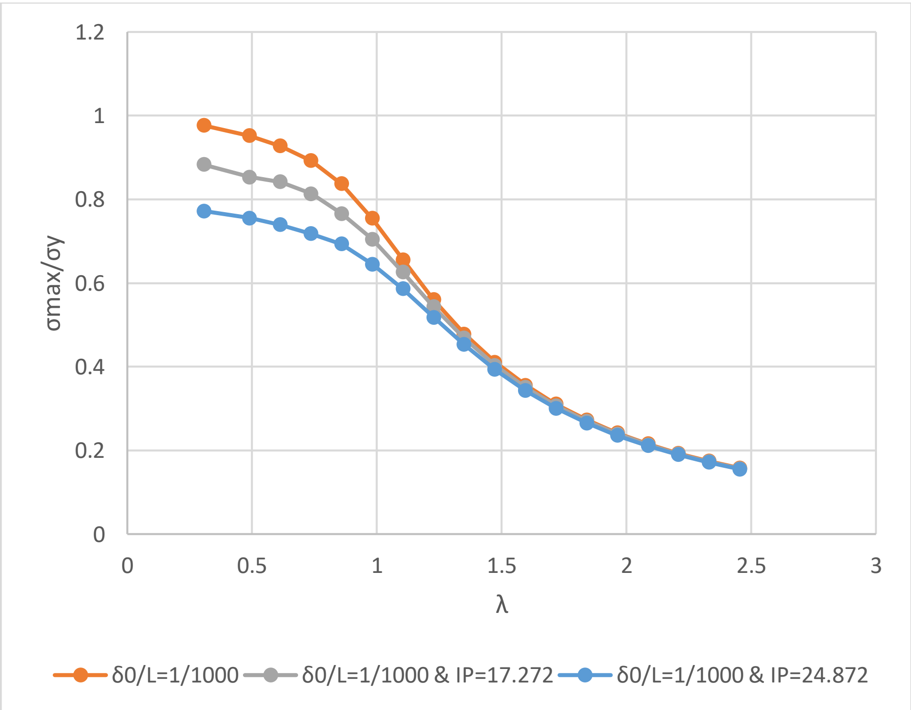

Figure 31: Normalized maximum Stress-Normalized Slenderness for imperfection amplitude L/1000 and IP=0, 17.272MPa and 24.872MPa

In the numerical analyses, it was observed that the buckling strength of tubular members is greater in the absence of internal pressure. When internal pressure is applied combined with the axial compressive loading, the buckling strength is significantly reduced especially for low and intermediate slenderness λ. In Figures 30 and 31, it is shown that as internal pressure increases, the buckling strength is reduced. However, it is also demonstrated that for high slenderness values, the presence of internal pressure doesn't affect the buckling strength so significantly and the curves tend to overlap. The results are consistent for both cases of imperfection amplitudes, L/2500 and L/1000.

4.1.3 Influence of Steel grade

To investigate the influence of material strength on the structural performance of members, a comparative study was conducted using two common Steel grades: Normal Steel S355 and High Strength Steel S700 across various global imperfection amplitudes and specifically L/5000, L/2500, L/1000 and L/500. The thickness in both cases is 15 mm. In Figure 32, the Normalized maximum Stress-Normalized Slenderness curves for S700 steel grade are plotted for the aforementioned imperfection amplitudes. In Figures 33,34,35 and 36, the Normalized maximum Stress-Normalized Slenderness curves are plotted per global imperfection amplitude, showing the effect of the two different Steel grades.

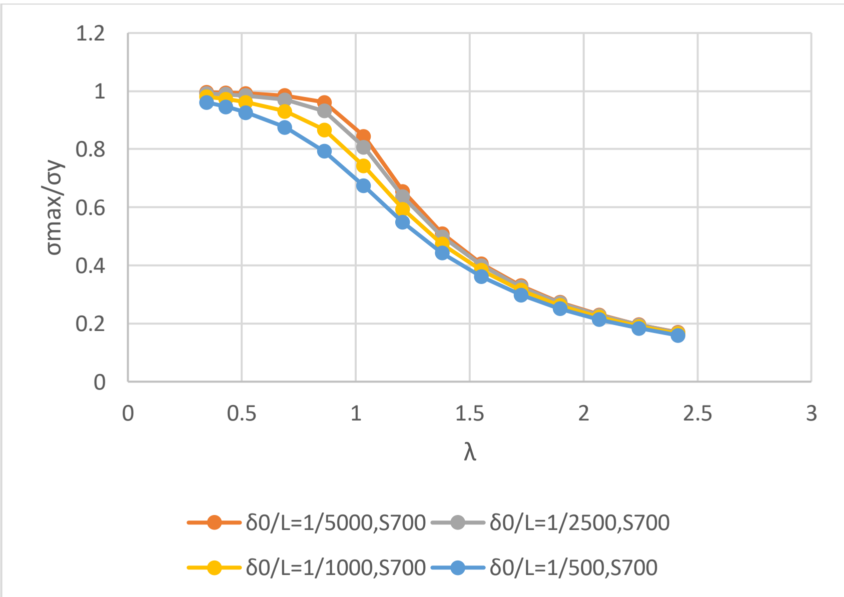

Figure 32: Normalized maximum Stress-Normalized Slenderness for L/5000, L/2500, L/1000, L/500 and Steel grade S700

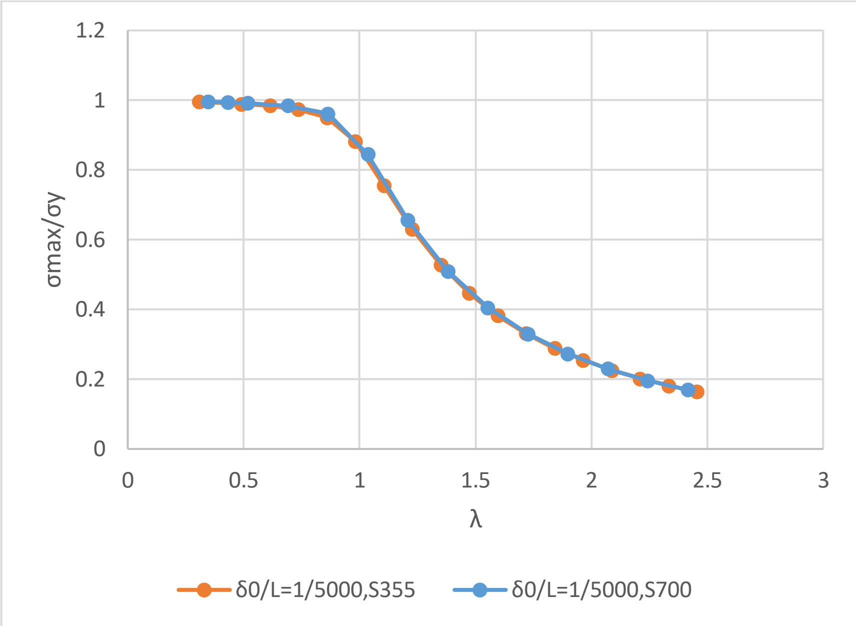

Figure 33: Normalized maximum Stress-Normalized Slenderness curve for imperfection amplitude L/5000 and Steel grades S355, S700

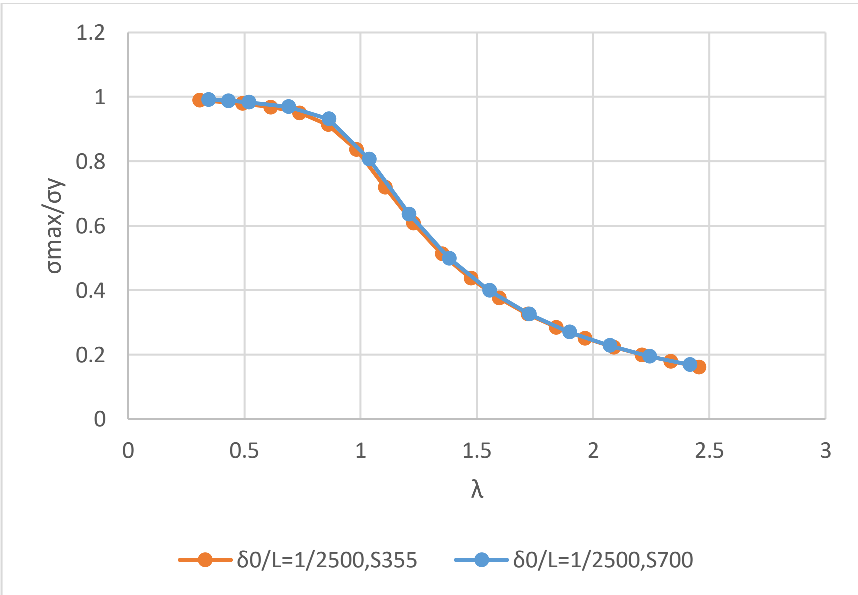

Figure 34: Normalized maximum Stress-Normalized Slenderness curve for imperfection amplitude L/2500 and Steel grades S355, S700

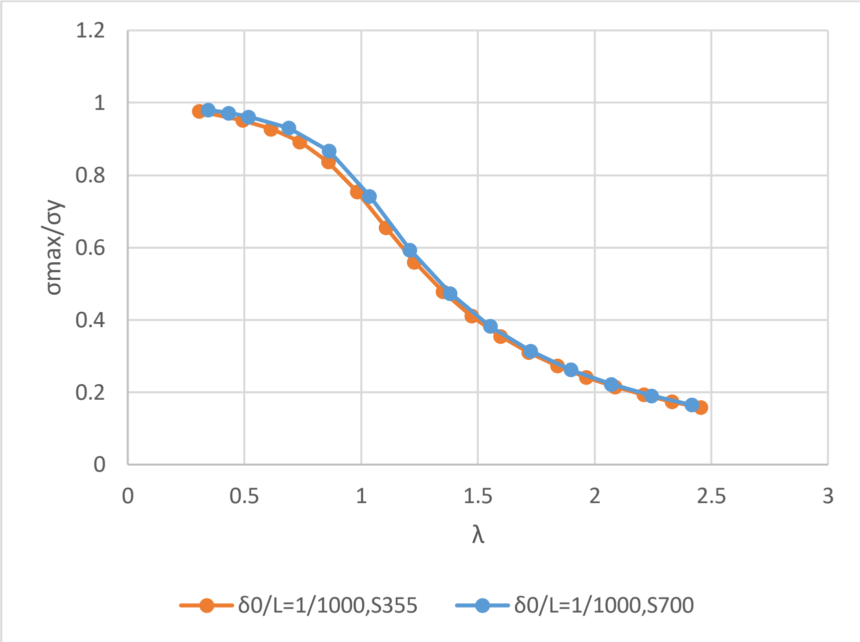

Figure 35: Normalized maximum Stress-Normalized Slenderness curve for imperfection amplitude L/1000 and Steel grades S355, S700

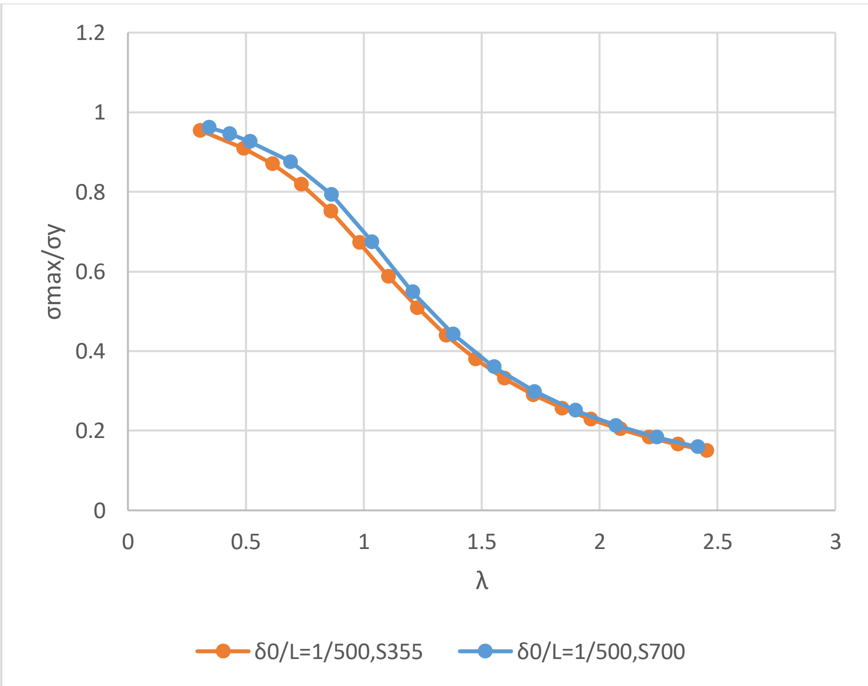

Figure 36: Normalized maximum Stress-Normalized Slenderness curve for imperfection amplitude L/500 and Steel grades S355, S700

The influence of material strength was investigated by comparing steel grades S355 and S700 across various initial imperfection amplitudes. The results are presented in terms of normalized maximum stress (σmax/σy) plotted against member slenderness λ, allowing for a direct comparison of structural performance independent of absolute yield strength. In Figure

32, it is shown that the normalized maximum strength of the columns is affected by the amplitude of global geometric imperfection and decreases with increasing global imperfection amplitude. This behavior was also observed for S355 steel grade. Then, comparing the two steel grades per global imperfection the following results are obtained. At low imperfection amplitudes L/5000 the two grades show nearly the same normalized responses across all slenderness values. This indicates that for very small imperfections the higher strength of S700 doesn't give much extra benefit once the results are normalized. However, as the imperfection amplitude increases the difference between the two grades becomes more noticeable. For bigger imperfection amplitudes, especially L/1000 and L/500, S700 has higher normalized maximum strength than S355, especially at moderate slenderness values. This suggests that high-strength steel is less sensitive to imperfections. At high slenderness values (above λ=2), both materials behave similarly again, showing that global buckling dominates and the steel grade is not significant when normalized maximum strength is evaluated.

4.1.4 Influence of thickness

The wall thickness of a circular hollow section (CHS) plays a crucial role in its buckling resistance. To assess this influence, the thickness is reduced to t=7.5 mm and the results are compared to those obtained with the previously assumed thickness t=15 mm, considering two global imperfection amplitudes: L/5000 and L/500. In Figures 37 and 38, the Normalized maximum Stress-Normalized Slenderness curves are plotted for the two imperfection amplitudes.

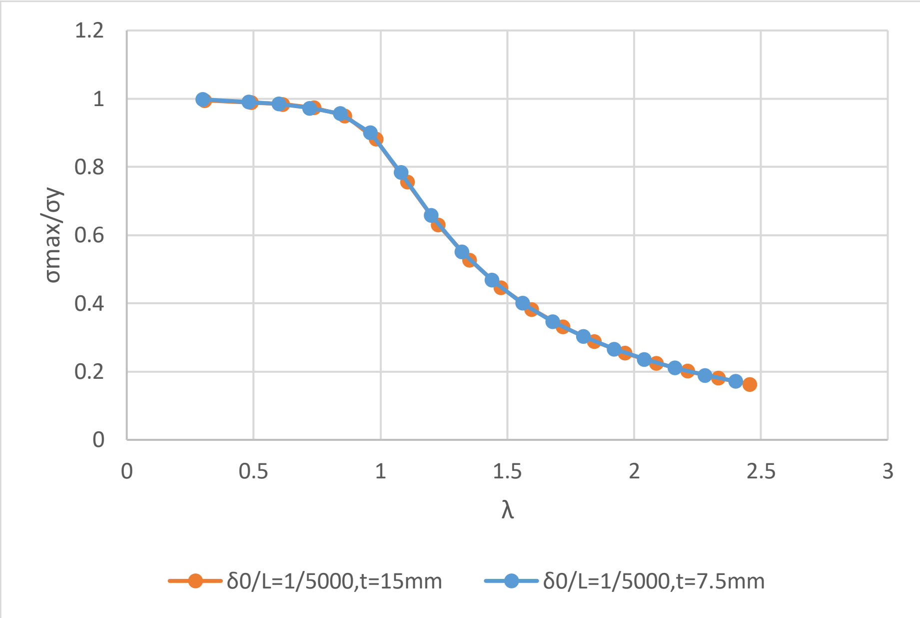

Figure 37: Normalized maximum Stress-Normalized Slenderness for imperfection amplitude L/5000 and two cases of thickness t=15 mm and t=7.5 mm

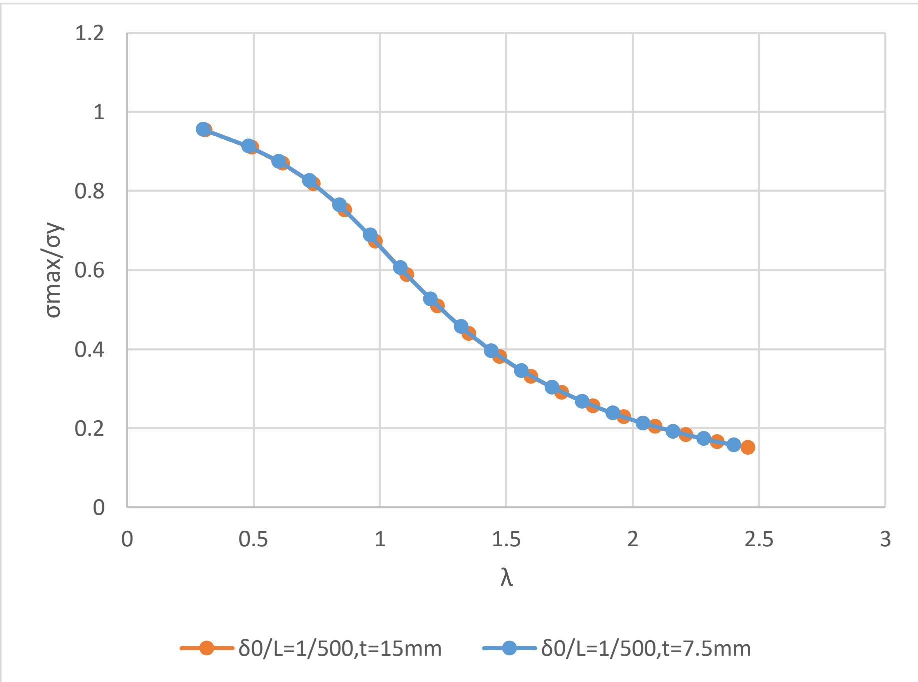

Figure 38: Normalized maximum Stress-Normalized Slenderness for imperfection amplitude L/500 and two cases of thickness t=15 mm and t=7.5 mm

The results show that the reduction of thickness from 15 mm to 7.5 mm does not lead to a noticeable change in the normalized maximum buckling stress. This outcome occurs because, when normalized maximum stresses are calculated and plotted versus normalized slenderness, the effect of thickness cancels out. For a reduced thickness, the Force decreases and the cross-sectional area A also decreases. As for the slenderness, the reduction in thickness leads only to a small change in value for the same length of member. This leads to stability curves that overlap. However, it is observed that when the thickness increases, the reaction force also increases. This can be shown in Figure 39, where for the same length, L=4000 mm and imperfection L/5000, the maximum reaction force is higher for greater thickness. The same results were obtained for all the lengths of tubular members that were modeled.

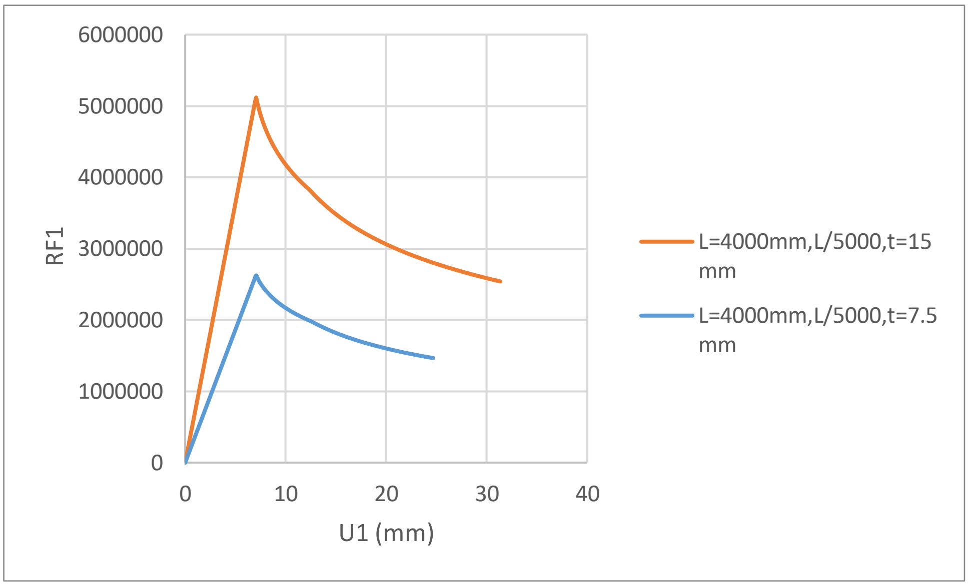

Figure 39: Force-Displacement curve for L=4000 mm, L/5000 and t=15 mm, t=7.5 mm

4.2 3D Model Results

Following the initial 2D Finite Element Analyses which provided efficient insight into the global buckling behavior of CHS columns, the 3D model results are now introduced. These 3D simulations allow for a more detailed representation of geometric imperfections and can sufficiently capture global and local buckling behavior.

In Figure 40, the initial local imperfection in the form of wrinkling scaled x10 is shown, while in Figure 41, the buckled shape of a tube of length L=4000 mm, t=3 mm, w=0.05t. In Figure 42, the buckled shape of a tube of length L=4000 mm, t=7.5 mm, w=0.05t is shown.

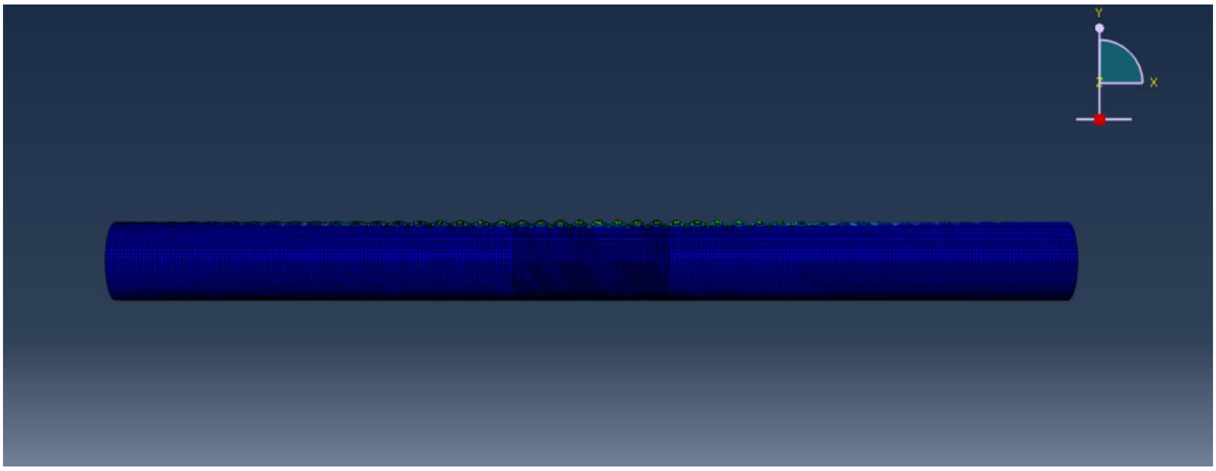

Figure 40: Local imperfection in the form of wrinkling scaled x10 for L=4000 mm, t=3 mm

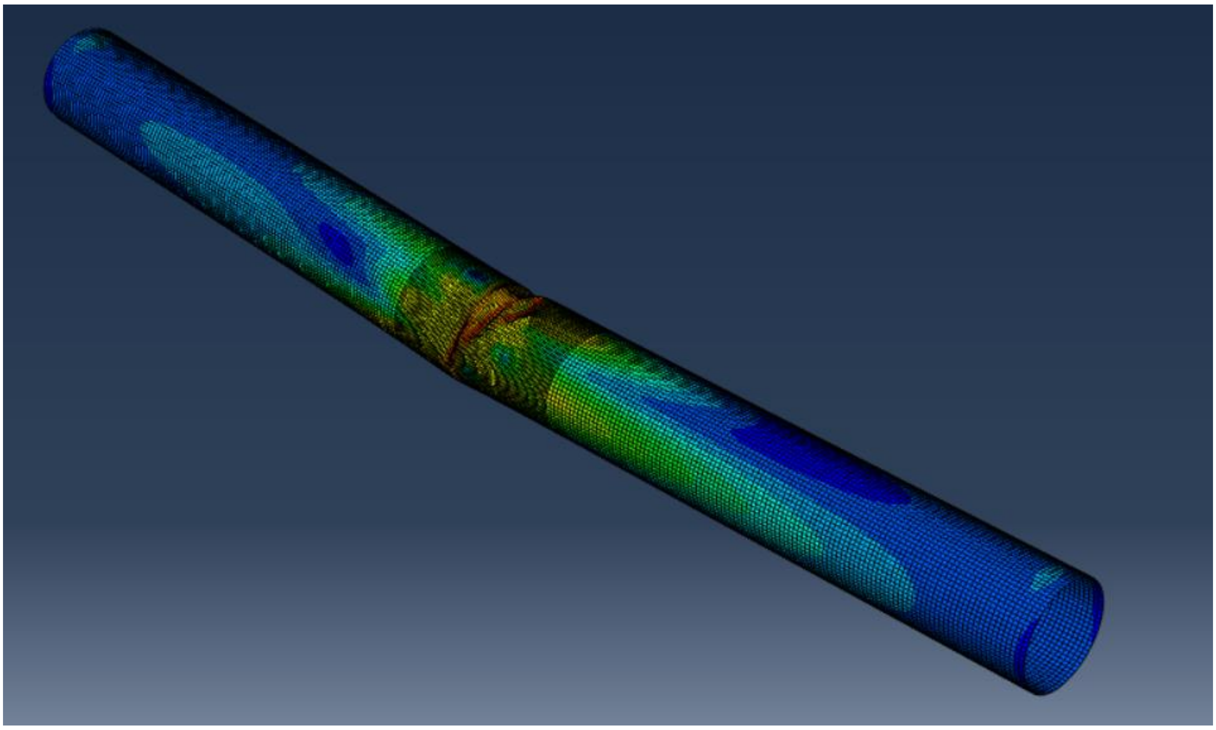

Figure 41: Buckled shape of tubular member of length L=4000 mm, t=3 mm, w=0.05t exhibiting a combination of Euler-type and shell-type buckling instability

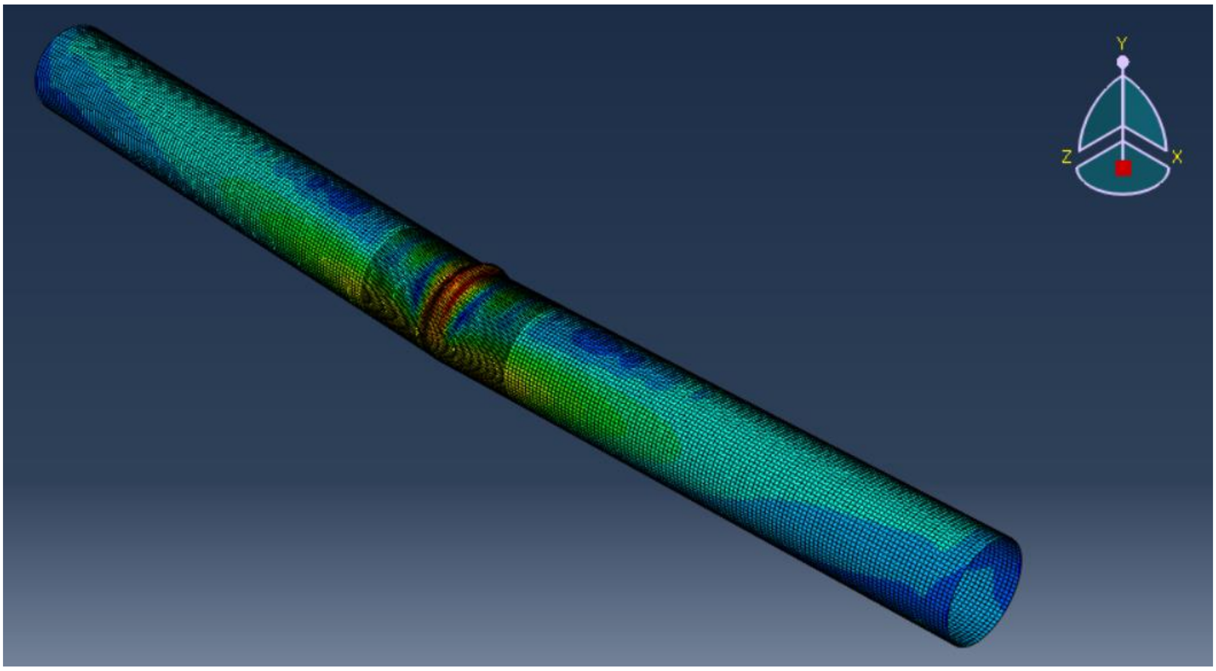

Figure 42: Failure mode of tubular member with L=4000 mm, t=7.5 mm, w=0.05t exhibiting an outward ring-type local buckle in the middle of the tube

4.2.1 Normalized Force-Displacement curves for D/t=43.18

In this section, the Normalized Force-Displacement curves are plotted for three different specimen lengths, 4000 mm, 8000 mm and 12000 mm and three magnitudes of initial local imperfection amplitudes w, corresponding to 5%, 10%, and 15% of thickness t. The thickness of the members is 7.5 mm and therefore the diameter-to-thickness ratio D/t=43.18. In Figure 43, the Normalized Force-Displacement for L=4000 mm and considering the three magnitudes of local imperfection amplitudes is plotted. Likewise, Figure 44 and Figure 45 are plotted for L=8000 mm and L=12000 mm respectively. To observe the effect of member slenderness on the buckling strength, a combined diagram for w=0.05t is shown in Figure 46.

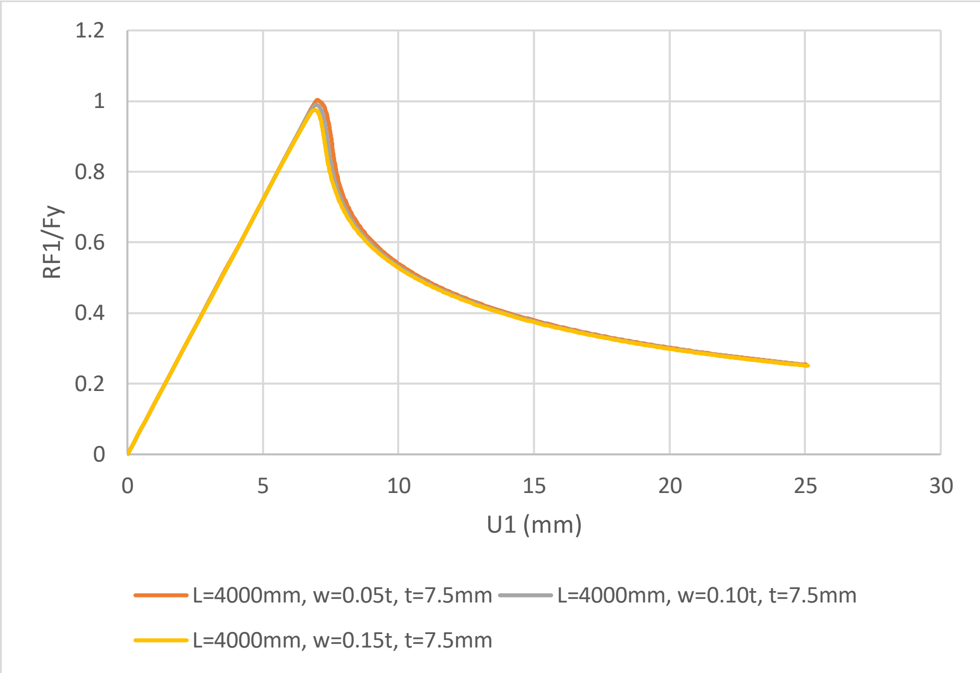

Figure 43: Normalized Force-Displacement for CHS 323.85x7.5 L=4000 mm and w=0.05t, 0.1t, 0.15t

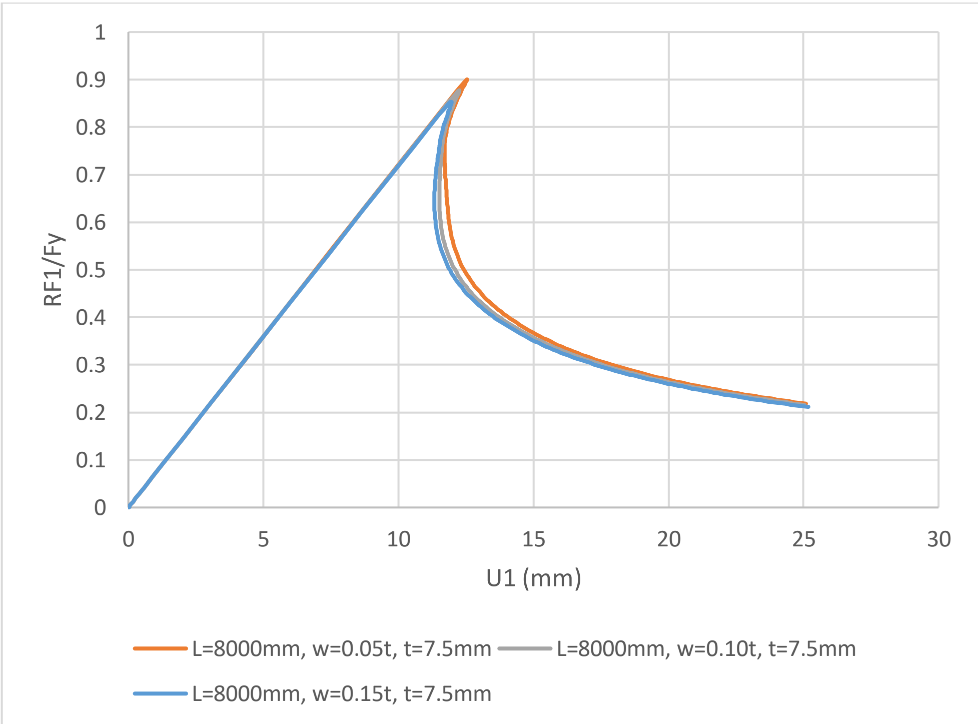

Figure 44: Normalized Force-Displacement for CHS 323.85x7.5 L=8000 mm and w=0.05t, 0.1t, 0.15t

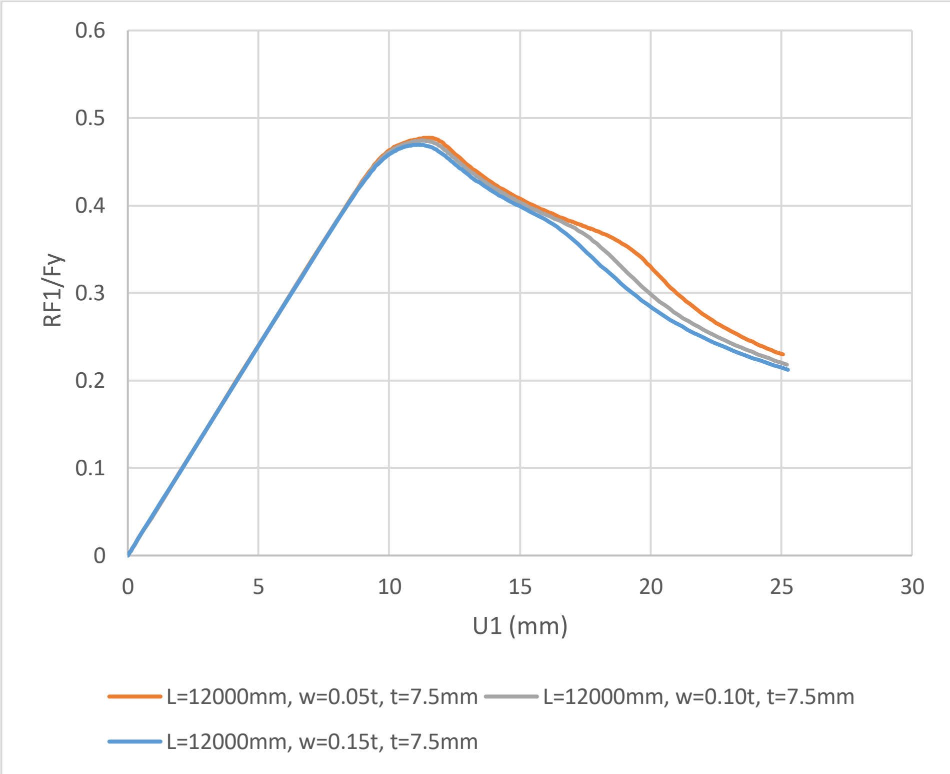

Figure 45: Normalized Force-Displacement for CHS 323.85x7.5 L=12000 mm and w=0.05t, 0.1t, 0.15t

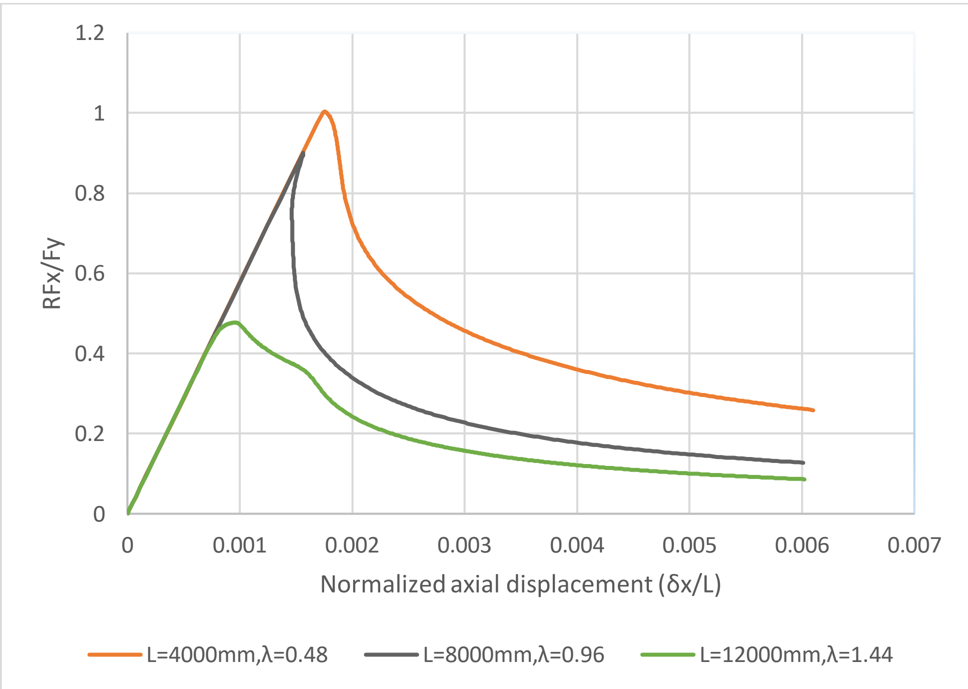

Figure 46: Normalized Force-Normalized axial displacement for the three member slenderness values and w=0.05t

The Force-Displacement curves, indicate that as the local imperfection amplitude increases, the maximum Reaction Force is reduced.

4.2.2 Comparison of 2D and 3D results for D/t=43.18

To observe the effect of the two different model approaches, 2D and 3D, a combined curve of Normalized maximum Stress-Normalized Slenderness for D/t=43.18 is plotted in Figure 47.

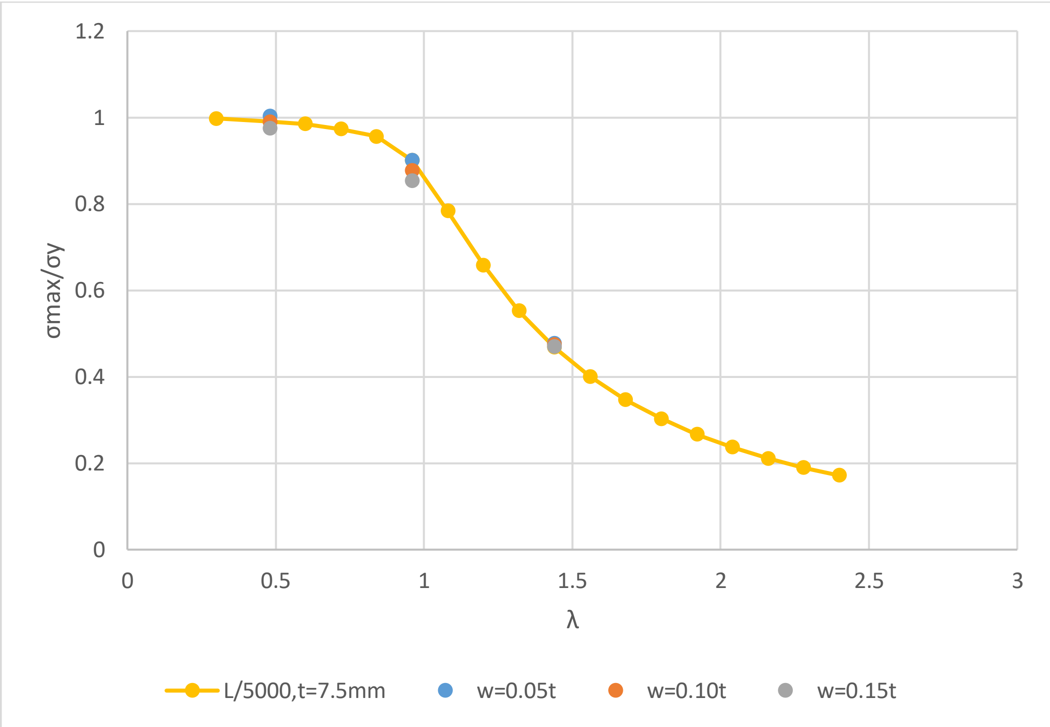

Figure 47: Normalized maximum Stress-Normalized Slenderness for t=7.5 mm, L/5000 and w=0.05t, 0.10t, 0.15t

The results indicate that for intermediate slenderness levels, specifically near 1, the local imperfection amplitude significantly influences the buckling strength of the tubular members. It is demonstrated that as the local imperfection amplitude increases, the buckling strength decreases. However, as slenderness increases and approaches 1.5, it is visible that the local imperfection does not reduce the buckling strength, meaning that global buckling governs the response. It can also be concluded that the 2D model approach is sufficient to capture the maximum buckling strength, but the local imperfection effects can only be observed in a full 3D model.

4.2.3 Normalized Force-Displacement curves for D/t=107.95

The cross-sectional geometry of the specimens is characterized by the diameter-to-thickness ratio D/t, which significantly influences their buckling and post-buckling behavior. A second case of thickness t=3 mm and D/t=107.95 is investigated. This corresponds to a thinner wall, more prone to local instabilities and imperfection sensitivity. The members length tested are also 4000 mm, 8000 mm and 12000 mm and the three magnitudes of initial local imperfection amplitudes w, are 5%, 10%, and 15% of thickness t. The Normalized Force-Displacement curves are shown in Figures 48, 49 and 50 for the three length cases and the local imperfection amplitudes.

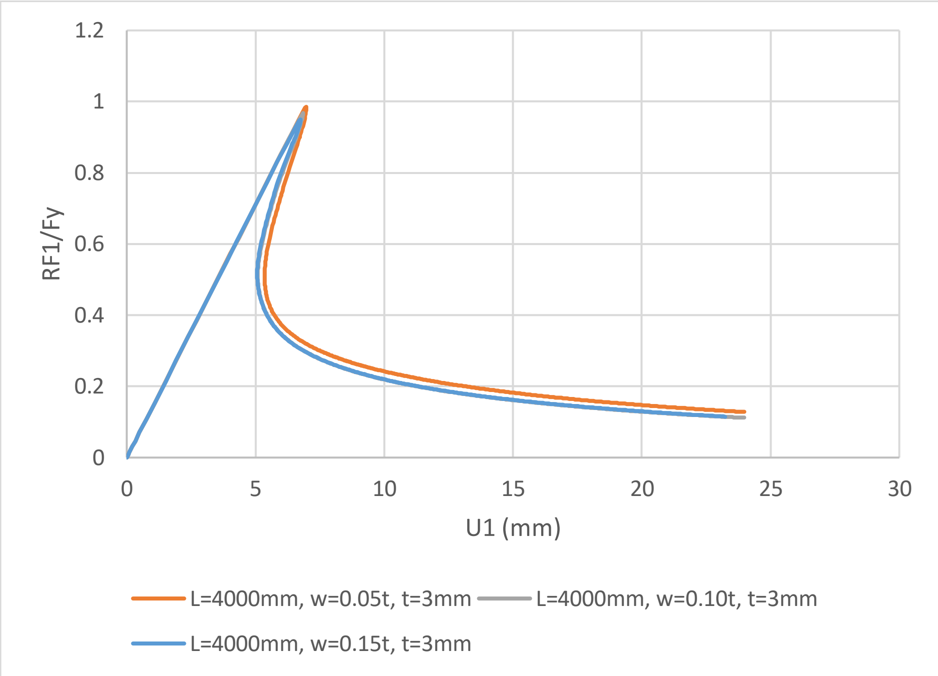

Figure 48: Normalized Force-Displacement for CHS 323.85x3 L=4000 mm and w=0.05t, 0.1t, 0.15t

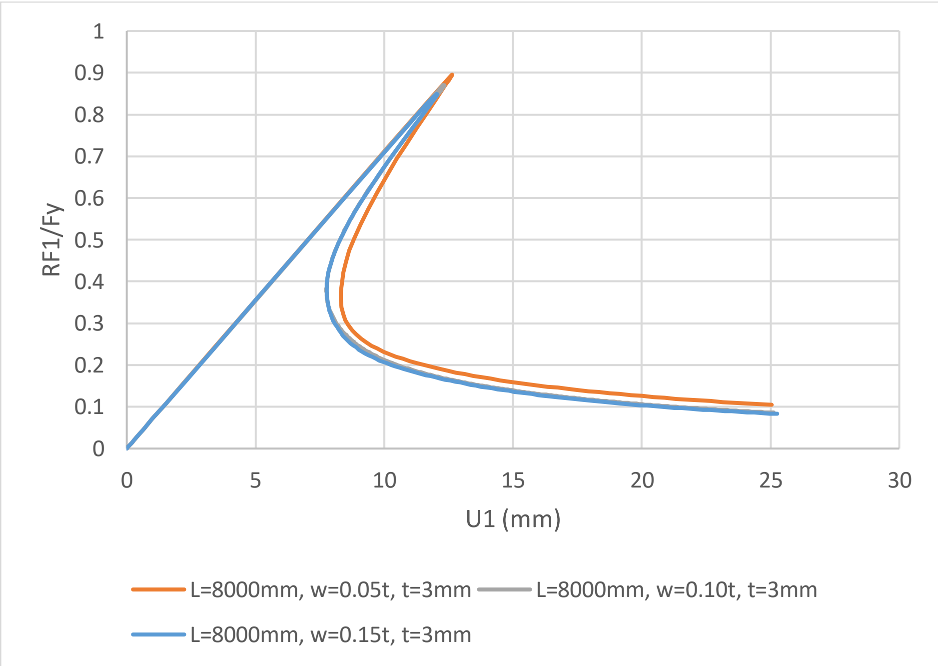

Figure 49: Normalized Force-Displacement for CHS 323.85x3 L=8000 mm and w=0.05t, 0.1t, 0.15t

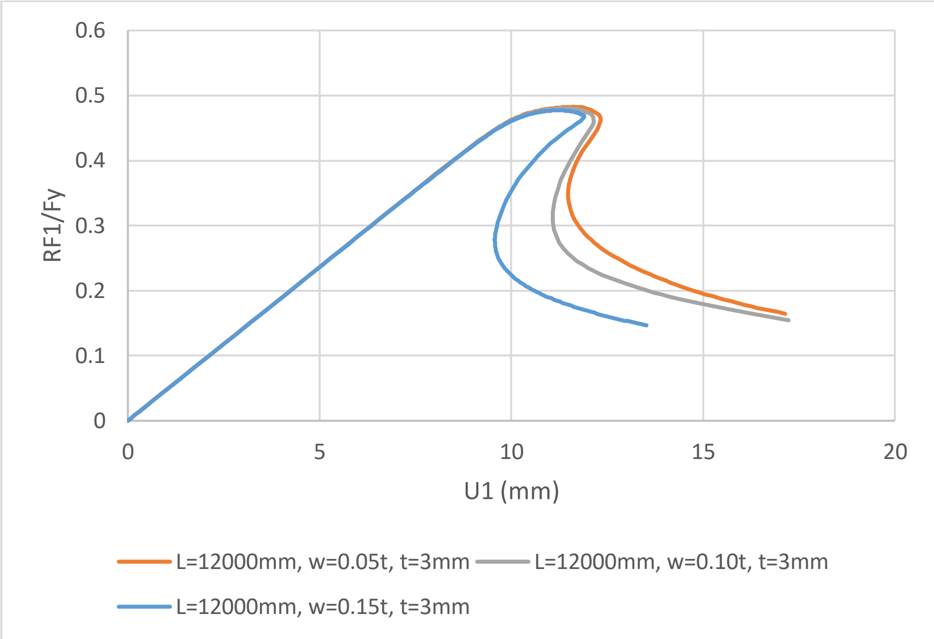

Figure 50: Normalized Force-Displacement for CHS 323.85x3 L=12000 mm and w=0.05t, 0.1t, 0.15t

The Force-Displacement curves, consistently with the results for t=7.5 mm, show that as the local imperfection amplitude increases, the maximum Reaction Force is reduced.

4.2.4 Comparison of 2D and 3D results for D/t=107.95

In Figure 51, a combined curve of Normalized maximum Stress-Normalized Slenderness for the case of D/t=107.95, consisting of 2D and 3D results, is plotted.

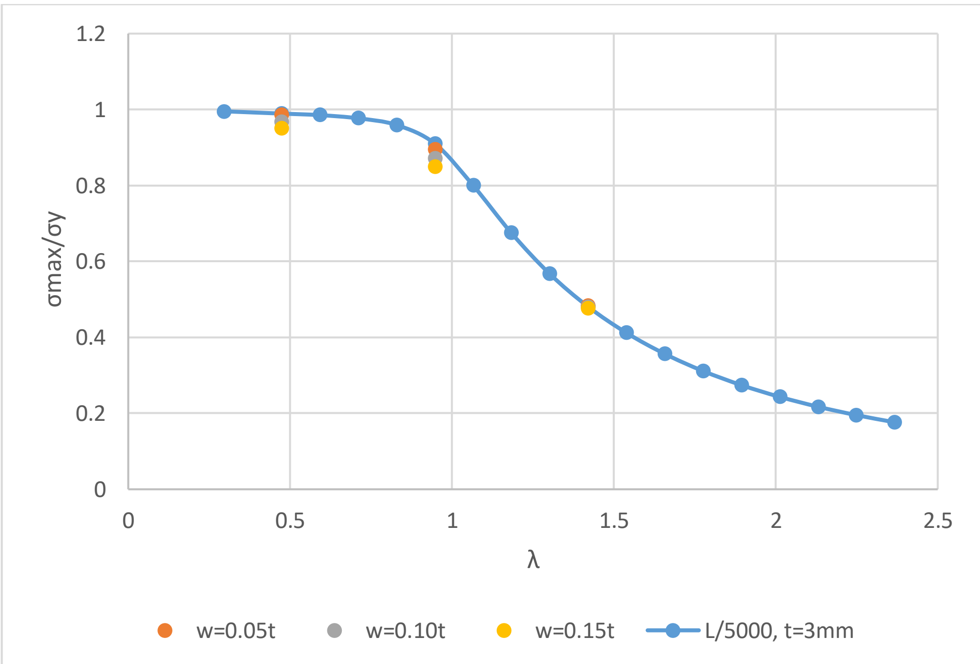

Figure 51: Normalized maximum Stress-Normalized Slenderness for t=3 mm, L/5000 and w=0.05t, 0.10t, 0.15t

The curve shows the results of normalized buckling strength for three slenderness cases and three local imperfection amplitudes, obtained from the 3D model, compared to the curve that occurred from the 2D model, without local imperfection integration. For tubular members with higher D/t ratios, even for stocky columns, in this case, slenderness approaching 0.5, the normalized buckling strength is reduced as the local imperfection amplitude increases. For intermediate slenderness values, near 1, it is shown that the effect is more pronounced. However, for more slender columns, as slenderness tends to 1.5, the local imperfection amplitude does not affect the buckling strength of the member. The curves almost overlap, indicating that the global buckling is more prominent.

Chapter 5. CONCLUSIONS – SUGGESTIONS FOR FURTHER STUDY

5.1 Conclusions

This thesis presented a numerical investigation of the buckling strength of circular hollow section (CHS) tubular members under axial compression, using finite element analysis (FEA).

The main conclusions drawn from this study can be summarized as follows:

1. **Influence of global imperfections**

- Initial global imperfections (out-of-straightness) have a major influence on the buckling resistance of the tubular members. It was overall observed that as the amplitude increases, the buckling strength is reduced.
- At low slenderness ratios, failure is governed by yielding, and the amplitude of imperfections has limited effect.
- At intermediate slenderness levels, imperfections markedly reduce axial capacity due to the interaction of yielding and global buckling.
- For very slender members, global buckling dominates the response and imperfections have only a small influence.

2. **Influence of Internal Pressure**

- The application of internal pressure in combination with axial compression reduces the buckling resistance of CHS members, particularly in stocky and moderately slender members.
- As Internal Pressure increases, the buckling strength is reduced.
- At higher slenderness values, the influence of internal pressure becomes negligible.

3. **Influence of Steel Grade**

- Both normal strength steel (S355) and high strength steel (S700) show similar behavior for small imperfection amplitudes.
- For larger imperfection amplitudes, high-strength steel (S700) exhibits reduced sensitivity to imperfections, achieving higher normalized resistance compared to S355, especially at intermediate slenderness values.

- At large slenderness values, both materials behave similarly and steel grade becomes less significant since the curves of S355 almost overlap with those of S700.

4. Influence of thickness

- The stability curves show that the reduction of wall thickness from t=15 mm to 7.5 mm does not lead to a difference in buckling strength of the members for both cases of global imperfection amplitude (L/5000 and L/500).
- However, as demonstrated in the force-displacement curve, when thickness is reduced, the reaction force is also reduced.

5. Comparison of 2D and 3D modeling approaches

- The 2D beam-column models are efficient for a first insight into the problem and provide accurate predictions of global buckling strength.
- The 3D shell models are essential for capturing local buckling and simulating the tubular members more realistically, which cannot be represented in simplified 2D analyses.
- Local imperfections are shown to reduce strength considerably in stocky and intermediate members. As the local imperfection amplitude increases, the maximum buckling strength is reduced.

5.2 Recommendations for further work

For further study, some interesting suggestions would be the following:

- The effects of combined loading cases (axial load and bending)
- Validation of the Numerical Results using the Eurocode 3 design rules or the American specification (AISC)
- Different types of initial imperfections
- Residual Stresses
- Rectangular Hollow Sections (RHS) and Elliptical Hollow Sections (EHS)

REFERENCES

[1] M. Rabi, F. P. V. Ferreira, I. Abarkan, V. Limbachiya, and R. Shamass, "Prediction of the cross-sectional capacity of cold-formed CHS using numerical modelling and machine learning," *Results in Engineering*, vol. 17, p. 100902, Mar. 2023, doi: 10.1016/J.RINENG.2023.100902.

[2] K.Ochi and B.S.Choo, "Ultimate strength and post-buckling behaviour of CHS columns - A comparison 404 between cold-formed and hot-finished sections," *Proceedings of the Fifth International Symposium on 405 Tubular Structures, Nottingham, United Kingdom*, pp. 163–170, 1993.

[3] Dundu Morgan and Chabalala Vongani, "Cold-formed circular hollow sections under axial compression," in *Construction Materials and Structures*, IOS Press, 2014, pp. 1148–1154. doi: 10.3233/978-1-61499-466-4-1148.

[4] H. G. L. Prion and P. C. Birkemoe, "Beam-Column Behavior of Fabricated Steel Tubular Members," *Journal of Structural Engineering*, vol. 118, no. 5, pp. 1213–1232, May 1992, doi: 10.1061/(ASCE)0733-9445(1992)118:5(1213).

[5] G. Shi, X. Jiang, W. Zhou, T. M. Chan, and Y. Zhang, "Experimental study on column buckling of 420 MPa high strength steel welded circular tubes," *J Constr Steel Res*, vol. 100, pp. 71–81, 2014, doi: 10.1016/j.jcsr.2014.04.028.

[6] A. E. Pournara, S. A. Karamanos, E. Mecozzi, and A. Lucci, "Structural resistance of high-strength steel CHS members," *J Constr Steel Res*, vol. 128, pp. 152–165, Jan. 2017, doi: 10.1016/j.jcsr.2016.08.003.

[7] S. Sun, Q. You, X. Gu, and Y. Peng, "Experimental and numerical investigation on global buckling of Q690 high strength steel tubes under axial compression," *IOP Conf Ser Mater Sci Eng*, vol. 774, no. 1, Mar. 2020, doi: 10.1088/1757-899X/774/1/012081.

[8] H. Wang, Y. Guo, Y. Bai, B. Zhang, Q. Sun, and J. Xue, "Experimental and numerical study on the stability capacity of Q690 high-strength circular steel tubes under axial compression," *International Journal of Steel Structures*, vol. 17, no. 3, pp. 843–861, Sep. 2017, doi: 10.1007/S13296-017-9001-1/METRICS.

[9] F. M. F. Shaker, K. Zarzor, S. Gaawan, A. Deifalla, and M. Salem, "Evaluation of Axial Compression Slenderness Limits of High and Ultra-High-Strength Steel Circular Hollow

Sections," *Buildings 2022, Vol. 12, Page 1093*, vol. 12, no. 8, p. 1093, Jul. 2022, doi: 10.3390/BUILDINGS12081093.

[10] X. Meng and L. Gardner, "Flexural buckling of normal and high strength steel CHS columns," *Structures*, vol. 34, pp. 4364–4375, Dec. 2021, doi: 10.1016/j.istruc.2021.09.106.

[11] C. Buchanan, E. Real, and L. Gardner, "Testing, simulation and design of cold-formed stainless steel CHS columns," 2018.

[12] M. Hayeck, J. Nseir, E. Saloumi, and N. Boissonnade, "Experimental characterization of steel tubular beam-columns resistance by means of the Overall Interaction Concept," *Thin-Walled Structures*, vol. 128, pp. 92–107, Jul. 2018, doi: 10.1016/J.TWS.2017.05.019.

[13] N. Europeenne and E. Norm, "EUROPEAN STANDARD Eurocode 3-Design of steel structures-Part 1-5: Plated structural elements," 2006.

[14] E. Norm, "EN 1993-1-12: Eurocode 3: Design of steel structures - Part 1-12: General - High strength steels," 2007.

[15] H. Fang, T. M. Chan, and B. Young, "Structural performance of cold-formed high strength steel tubular columns," *Eng Struct*, vol. 177, pp. 473–488, Dec. 2018, doi: 10.1016/J.ENGSTRUCT.2018.09.082.

[16] X. Meng and L. Gardner, "Stability and design of normal and high strength steel CHS beam-columns," *Eng Struct*, vol. 251, Jan. 2022, doi: 10.1016/J.ENGSTRUCT.2021.113361.

[17] "(EN 1993-1-1) Eurocode 3: Design of steel structures - Part 1-1: General rules and rules for buildings," 2005.

[18] "Abaqus 2016, SIMULIA - Dassault Systèmes," 2016.

[19] X. Meng, L. Gardner, A. J. Sadowski, and J. M. Rotter, "Elasto-plastic behaviour and design of semi-compact circular hollow sections," *Thin-Walled Structures*, vol. 148, Mar. 2020, doi: 10.1016/J.TWS.2019.106486.

[20] J. M. Rotter, A. J. Sadowski, and L. Chen, "Nonlinear stability of thin elastic cylinders of different length under global bending," *Int J Solids Struct*, vol. 51, no. 15–16, pp. 2826–2839, Aug. 2014, doi: 10.1016/J.IJSOLSTR.2014.04.002.